Global Analytical Potential Hypersurface for Large Amplitude Nuclear Motion and Reactions in Methane II. Characteristic Properties of the Potential and Comparison to Other Potentials and Experimental Information†

Roberto Marquardt*

Laboratoire de Chimie Theorique, Université de Marne-la-Vallée, 5 Bd Descartes (Champs-sur-Marne), F-77454 Marne-la-Vallée CEDEX 2, France

Martin Quack*

Physical Chemistry, ETH Zürich, CH-8093 Zürich, Switzerland

Received: October 31, 2003

The global analytical potential surface for the electronic ground state of methane developed in paper I is analyzed and discussed in detail. A new determination of the experimental potential surface for the CH chromophore in CHD_3, obtained from more recently measured line positions and integrated absorption coefficients, is also reported. The complete, nine-dimensional calculation of the vibrational ground state by diffusion quantum Monte Carlo on the fully anharmonic potential surface allows the determination of $r_e = (1.086 \pm 0.002)$ Å with a high level of certainty from comparison with experimental values of rotational constants for methane and isotopomers. Other results regarding properties of the anharmonic potential surface close to the equilibrium configuration are theoretical values for the vibrationally induced electric dipole moments in CH_3D, CH_2D_2, and CHD_3, which are obtained in conjunction with a nine-dimensional, vector-valued representation of the electric dipole moment in this molecule and agree well with the experimental data. It is shown that, if equilibrium geometry and harmonic force field are fixed to experimental values, the overtone spectrum of the CH chromophore in CHD_3 can be described in an acceptable way ($\langle|\tilde{\nu}_{cal} - \tilde{\nu}_{obs}|\rangle \approx 40$ cm^{-1} up to 18 000 cm^{-1} (METPOT 3). The agreement can be improved to within 17 cm^{-1} (METPOT 4), on the average, if the anharmonic part of the model potential is refined with data from the experimentally derived, three-dimensional CH chromophore potential surface from Lewerenz and Quack (*J. Chem. Phys.* **88**). For this purpose, the analytical representation of the potential, mainly along the bending degrees of freedom, must be sufficiently flexible, as shown by the present calculations. The accuracy regarding the description of spectroscopic data pertaining to highly excited vibrational states and the global character of the proposed potential surface representation render it a powerful instrument for the theoretical treatment of chemical reaction dynamics. A relation to reaction kinetics can be established through calculation of the lowest adiabatic channel on the complete nine-dimensional potential hypersurface for methane using quasiadiabatic channel quantum Monte Carlo techniques. It is found that the behavior of this channel, corresponding approximately to an exponential interpolation with a parameter $\alpha \approx 0.7-0.8$ Å^{-1} in the adiabatic channel model, is consistent with empirical results obtained from experiment. Further refinements of the models are feasible and expected, when full dimensional calculations of the solution of the rovibrational Schrödinger equation will be performed.

1. Introduction

The ab initio calculation of anharmonic potentials by analytic derivative methods for the dynamics of polyatomic molecules has introduced a new dimension to quantum chemistry.[1] These methods usually characterize the potential in regions not too far from the equilibrium geometry or around certain well-defined stationary points or reaction paths. Another approach would be to generate global analytical descriptions of potential hypersurfaces, which are qualitatively and quantitatively adequate for very large amplitude motions, including intramolecular rearrangement processes. We have in recent years generated such potentials for a number of prototypical molecular systems, and the potential hypersurface and dynamics of methane is a particularly interesting example because of its fundamental importance in chemistry, ranging from combustion to astrophysics (see refs 2 and 3 and references therein, hereafter called paper I). In paper I,[3] the analytical representation of a global potential-energy surface for the electronic ground state of methane was developed and parameter values were determined by adjustment to an ab initio data set under special consideration of additional experimental constraints. In the present paper, a more detailed analysis of our first results is carried out by comparison with experimental information from thermochemical, kinetic, and spectroscopic data. The methods used include full dimensional diffusion quantum Monte Carlo[4,5] and quasiadiabatic channel quantum Monte Carlo calculations[4] and bound-states quantum dynamics in reduced subspaces.[6]

These methods have been used before in connection with the discussion of previous model potentials (METPOT 1 and

† Part of the special issue "Fritz Schaefer Festschrift".

* Authors to whom correspondence may be addressed. E-mail: roberto.marquardt@univ-mlv.fr (R.M.); Martin@Quack.ch (M.Q.).

10.1021/jp037305v CCC: $27.50
Published on Web 04/08/2004

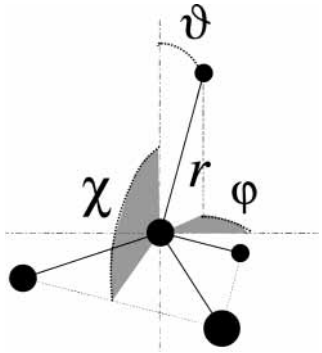

Figure 1. Definition of internal coordinates used for the ab initio calculations and the representation of the potential hypersurface in CH_4.

METPOT 2 in ref 3). Here, the discussion is extended to further developed model potentials METPOT 3 and METPOT 4, which will be compared, in graphical representations, to the ab initio data used in paper I and to some widely used potentials from the literature.[7−9] Other potentials have been discussed in refs 3 and 10.

METPOT 4 differs from METPOT 3 essentially by an additional experimental refinement of the global potential surface with respect to the reduced space potential of the CH chromophore in CHD_3. We used this potential, in the form first derived by Lewerenz and Quack,[6] as an additional source of data points for the adjustment of parameter values. We also discuss a new determination of the experimental CH chromophore potential under inclusion of more recent data from high resolution spectroscopy and the experimental, full-dimensional dipole-moment function for methane, which was determined previously.[11]

After the present work has been underway for some time and the initial parts published,[2,3,5,11] there has been also some additional effort on characterizing the nine-dimensional potential of methane as well as on full-dimensional calculations of vibrational energy levels on such potentials.[12−16] Our work should be seen in relation to recent calculations on the wave packet dynamics in methane isotopomers.[17,18] Figure 1 shows the coordinates used to describe analytically the potential surface of methane in the present work.

2. Theory

The diffusion quantum Monte Carlo (DQMC) method for the full dimensional solution of the Schrödinger equation has been described previously (ref 5 and references therein). Basically, the Schrödinger equation is interpreted as a diffusion equation with a sink term given by the potential, and the energy of a stationary state is estimated from a weighted average $\bar{V}$ of the potential energy with weights from the (positive) stationary wave function ψ after sufficiently long propagation time. At present, we have limited the calculation to the ground state ψ_0, although extensions to excited states are feasible, in principle (refs 4, 19−21 and references therein). Given the simulation of the ground-state wave function ψ_0, expectation values $\bar{O} \equiv \langle\psi_0|\hat{O}|\psi_0\rangle$ of any multiplicative operator $\hat{O}$ may be derived by defining $\hat{H}_\lambda = \hat{H}_0 + \lambda\hat{O}$. If E_λ is the ground-state energy associated to $\hat{H}_\lambda$, as was shown in ref 5, that $\bar{O}$ is given by the intercept of $(E_\lambda - E_{-\lambda})/(2\lambda)$ at $\lambda = 0$. This is also used in the present article to calculate the expectation values of rotational constants $(A + B + C)/3$ (with $\lambda = J(J + 1)$) and of the vibrationally induced permanent dipole moment μ_0^α (with $\lambda = -\epsilon^\alpha$, where ϵ^α is an electric field component along the molecule fixed direction α) in section 3.6 below. For the electric dipole-moment operator, the expression derived in ref 11 was used

$$\vec{\mu} = \sum_{i=1}^{4} \frac{\vec{x}_i}{r_i} \mu_b(r_i,\alpha_{ij},\alpha_{ik},\alpha_{il}) \quad (1)$$

where $\vec{x}_i$ is the bond vector from the central carbon atom to the ith hydrogen atom (or its isotope), $r_i = |\vec{x}_i|$, and μ_b is a generalized bond dipole function which depends on r_i and on the three neighboring valence angles α_{ij}, α_{ik}, α_{il} for $j, k, l \neq i$

$$\mu_b(r_i,\alpha_{ij},\alpha_{ik},\alpha_{il}) = [\mu_b^0 + \mu_b^1(r_i - r_e) + \mu_b^2(r_i - r_e)^2 + \mu_b^3(r_i - r_e)^3 + \mu_a^1(\cos(\alpha_{ij}) + \cos(\alpha_{ik}) + \cos(\alpha_{il}) + 1) + \mu_a^2((2\cos(\alpha_{ij}) - \cos(\alpha_{ik}) - \cos(\alpha_{il}))^2 + 3(\cos(\alpha_{ik}) - \cos(\alpha_{il}))^2)]\exp(-\beta^2(r_i - r_e)^2) \quad (2)$$

The parameter values determined in ref 11 are: $\mu_b^0 = 0.4$ D, $\mu_b^1 = -0.7$ D Å^{-1}, $\mu_b^2 = -0.7744$ D Å^{-2}, $\mu_b^3 = -0.1079$ D Å^{-3}, $\beta = 0.8922$ Å^{-1} $\mu_a^1 = 0.0570$ D, $\mu_a^2 = 0.0243$ D, and $r_e = 1.0858$ Å.

Quasiadiabatic channel quantum Monte Carlo calculations are diffusion quantum Monte Carlo calculations performed at fixed values of one or more coordinates, e.g., the CH bond length r(CH) ("clamped DQMC" [4,19,21]). Here, they yield the fully anharmonic zero-point energy in the reduced space of coordinates where r(CH) has been excluded. Subsequent variation of r(CH) yields a function $V_{adi}(r)$, which corresponds to the lowest quasiadiabatic channel for the dissociation reaction

$$(^1A_1)CH_4 \rightarrow (^2A''_2)CH_3 + (^2S_{1/2})H \quad (3)$$

in methane. Let $V_{rel}(r)$ be the (electronic) potential surface at $r = r$(CH) with relaxed motion of the CH_3 frame. The difference $\Delta V(r(CH)) \equiv V_{adi}(r(CH)) - V_{rel}(r(CH))$ can be described by an empirical model with exponential decay (from ref 22, eq 13, see also refs 23 and 24), which is given here in the logarithmic form

$$\ln\left(\frac{\Delta V(r) - \Delta V(\infty)}{\Delta V(r_e) - \Delta V(\infty)}\right) = -\alpha(r - r_e) \quad (4)$$

Here, $\Delta V(\infty) = \Delta V(r(CH) = \infty)$ is the zero-point energy of the methyl radical. This model will be discussed in section 3.2 below.

Reduced space quantum dynamics has been used to treat the dynamics of the CH chromophore in CHXYZ compounds (see, e.g., refs 6, 25−27). The model introduced by Lewerenz and Quack[6] uses the function

$$V_{CH}^{LQ} = \frac{1}{2}\omega_s y^2 + \frac{1}{2}K_{\phi\phi}\phi^2 + K_{\phi\phi\phi\phi}\phi^4 + K_{\rho\phi\phi}y\phi^2 + K_{\rho\rho\phi\phi}y^2\phi^2 \quad (5)$$

where $y = (1 - \exp(-a\rho))/a$, $a = ((2x_s/33.715262\ \text{cm}^{-1}))^{1/2}(u)^{1/2}$ Å^{-1}, and $\rho = (Q_b^2 + (Q_s + \rho_0)^2)^{1/2} - \rho_0$, $\phi = \arctan(Q_b/(Q_s + \rho_0))$ (see also eq 8 in ref 6). Q_s is the stretching and $Q_b \equiv (Q_{b_1}^2 + Q_{b_2}^2)^{1/2}$ is the isotropic bending normal coordinate. The parameters in eq 5 may be determined from a direct adjustment to spectroscopic line positions and intensities from experiment.

We may also consider the chromophore potential V_{CH}^{LQ} as a two- or three-dimensional cut of the total potential surface, defined in normal coordinates. The total potential surface is normally represented in internal, curvilinear coordinates, such as in eq 4 in paper I. These may, however, be written as

functions of Cartesian coordinates of the nuclei, which are linear functions of the normal coordinates, essentially determined by the harmonic force field and equilibrium structure.[28] The effective potential in normal coordinates is then given by the electronic potential (in the Born−Oppenheimer approximation) and a pseudopotential, which results from the transformation of space fixed to molecule fixed, rotating Cartesian coordinates.[29] The latter is almost constant in the relevant regions of vibrations of the CH chromophore. For the electronic part, we may write

$$V_{CH}^{LQ}(Q_s, Q_{b_1}, Q_{b_2}) = V(Q_1 = Q_s, Q_5 = Q_{b_1}, Q_6 = Q_{b_2}, Q_2 = ... = Q_9 = 0) \quad (6)$$

where V may be given by eq 4 in paper I, and Q_1 is the normal coordinate of the CH stretching vibration, with wavenumbers close to 3000 cm^{-1}, and Q_5 and Q_6 are the normal coordinates for the bending vibrations in CHD_3 (at ∼1300 cm^{-1}) ($Q_6 = Q_{b_2}$ being the A'' mode in C_s symmetry). Potential cuts along these coordinates are shown below in the parts a and b of Figure 10 as equidistant curves of equal potential (contour plots). The potential is nearly isotropic in molecules of the type CHX_3[30] (cf. Figure 10a, the anisotropy along Q_{b_2} being hardly distinguishable), which means that the potential in eq 6 is nearly a function of Q_b only.

Another possibility is to interpret V_{CH}^{LQ} as a quasiadiabatic potential

$$V_{CH}^{LQ}(Q_s, Q_{b_1}, Q_{b_2}) = \langle \Psi | V(Q_1 = Q_s, Q_5 = Q_{b_1}, Q_6 = Q_{b2}, Q_2, ..., Q_9) | \Psi \rangle \quad (7)$$

where Ψ was simulated within the "clamped DQMC" formalism[4,19,21] at fixed values of the coordinates Q_1, Q_5, and Q_6. This approach corresponds to the interpretation of the CH chromophore potential as a quasiadiabatic channel potential by explicitly considering the vibrational zero-point energy of the frame modes, rather than a "sudden" potential, with "frozen" frame vibrations, such as eq 6.

3. Results and Discussion

3.1. Potential along a CH Bond Length. The potential as a function of a CH bond length is shown in Figure 2a, in which the CH_3 frame is kept at the pyramidal structure from the CH_4 equilibrium ($\chi = 109.47°$, see the definition of χ in Figure 1). In Figure 2b, CH_3 is in the planar equilibrium structure of the methyl radical. These functions correspond essentially to the potential for the dissociation reaction, eq 3. We recognize, first, the importance of using Morse or "Morse-type" potentials (this work and DHS)[8] for the qualitatively correct description of the dissociative behavior and the limits for the validity of quartic force fields (GR[7] and LMT).[9]

The dissociation energy (D_e) from ref 8 is roughly 1000 cm^{-1} too low compared to the present result, which corresponds to the "experimental" value of 0.783 aJ (∼39 500 cm^{-1}), obtained from $D_0 = 0.717$ aJ (431.8 kJ mol^{-1} [31,32]) and the zero-point correction (harmonically). The uncertainty of D_e is estimated to be ±300 cm^{-1} (0.0060 aJ ≈ 1 kcal mol^{-1} "chemical accuracy"). In ref 32, the uncertainty of D_0 is given as ±0.4 kJ mol^{-1} (∼0.0007 aJ) and a more recent determination gives $D_0 = (4.487 \pm 0.001)$ eV, or (432.93 ± 0.10) kJ mol^{-1}.[33] In addition, there may be significant errors originating from the estimation of the zero-point energies of CH_4 and CH_3. In Table 3, we give values for these energies obtained both in the harmonic approximation and from the solution of the Schrödinger equation for the nuclear motion in the complete, nine-dimensional anharmonic potential models of the present work, with the diffusion quantum Monte Carlo algorithm (DQMC).[4,5] The zero-point energy difference is 3332 cm^{-1} in the harmonic approximation and roughly 3270 cm^{-1} from the DQMC calculations (both for METPOT 3 and METPOT 4). The relatively small difference of roughly 60 cm^{-1} between the harmonic and anharmonic calculations does not, in general, justify the harmonic approximation for the determination of D_e from experimental data, since there is an obviously large compensation of errors. In the present case, however, it allowed for a preliminary realistic estimation of D_e. The anharmonicity of the strongly binding stretching potential was assumed here to be similar for CH_4 and CH_3, which needs, however, to be confirmed with more detailed ab initio calculations to map the potential surface of the methyl radical. The anharmonic force field of CH_3 needs also to be determined with more certainty from experiment.[34,35]

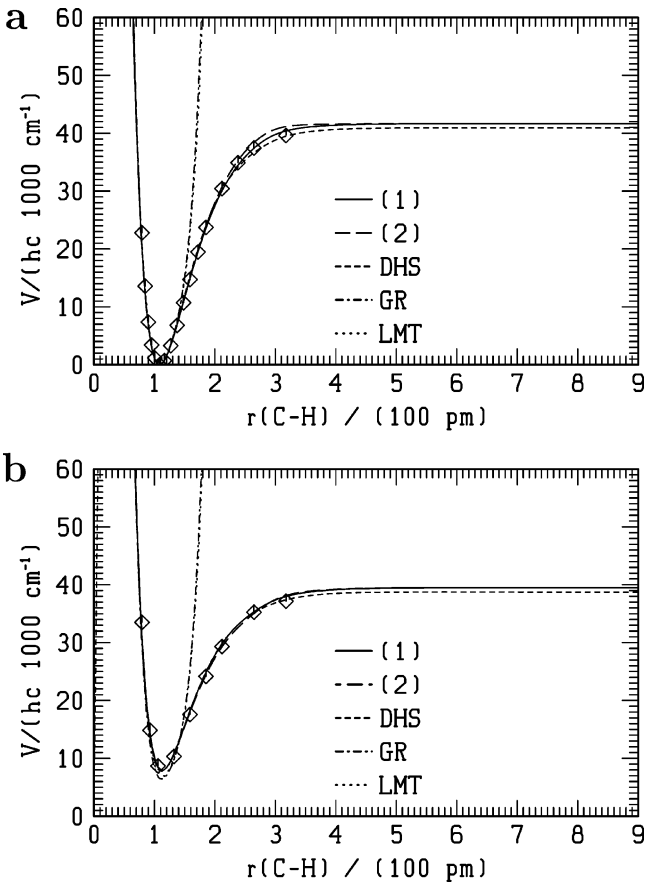

Figure 2. (a) Potential along r(CH) with pyramidal CH_3 frame ($\chi = 109.47°$, see Figure 1). Continuous curve (1) = METPOT 3, long-dashed curve (2) = METPOT 4, DHS is from ref 8, GR is from ref 7, LMT is from ref 9, and ◇ is from refs 6 and 36. (b) Potential along r(CH) with planar CH_3 frame ($\chi = 90°$); continuous curve (1) = METPOT 3, long-dashed curve (2) = METPOT 4, DHS is from ref 8, GR is from ref 7, LMT is from ref 9, and ◇ is from refs 6 and 36. METPOT 3 and METPOT 4 are hardly distinguishable here.

From the representations METPOT 3 and 4, the dispersion constant C^I for methane is given by $C^I = F_s(1)\epsilon_6(1)r_s(1)^6 \approx 0.72$ aJ Å^6 (see eq 6 in paper I). From a direct fit of the formula $V_{s(XY)} \sim D_e^I - (C^I/r_i^6)$ to the ab initio data from ref 36 in the asymptotic region r(CH) → ∞, the value $C^I \approx 0.66$ aJ Å^6 is obtained.

The energy difference between planar and pyramidal CH_3 frames at the methane equilibrium bond length is roughly 7950

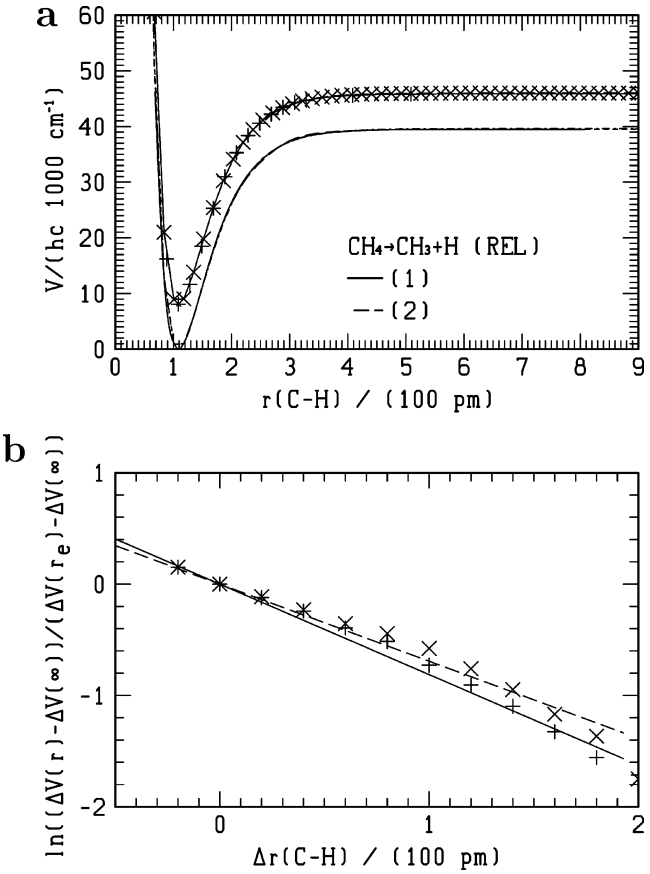

Figure 3. (a) Lower continuous curve: potential $V_{rel}(r(CH))$ along $r(CH)$ with relaxed CH_3 frame ($\cos(\chi)$ roughly as given in eq 22 of paper I). Lower broken curve: Morse potential fitted to $V_{rel}(r(CH))$. Marked points: "clamped DQMC" energies (see text); + = METPOT 3, × = METPOT 4. Upper curves: Morse potentials fitted to the DQMC points. The continuous curve (1) = METPOT 3 and the long-dashed curve (2) = METPOT 4 are hardly distinguishable. (b) Adjustment of the exponential interpolation parameter in the lowest quasiadiabatic channel for the methane dissociation reaction (see also eq 4). + = METPOT 3 (continuous line); × = METPOT 4 (broken line).

cm^{-1}. For the isolated methyl radical it is 2300 cm^{-1} (at $\chi = 109.47°$, the vertical distance of the H_3 plane from equilibrium is $z \approx 0.36$ Å), which agrees well with results from Figure 4 of ref 37.

3.2. Lowest Quasiadiabatic Channel. The potential $V_{rel}(r(CH))$, calculated as a function of one CH bond length while the CH_3 frame is allowed to relax, is shown in Figure 3a (lower curves, both for METPOT 3 and METPOT 4, which can hardly be distinguished). On top of it, the broken curves show the results of a Morse potential fit to $V_{rel}(r(CH))$ with parameters $\tilde{D} = 39572(39618)$ cm^{-1} and $a = 1.833(1.825)$ $Å^{-1}$ (for METPOT 3; values for METPOT 4 in parentheses). At fixed values of $r(CH)$, "clamped DQMC" calculations have been performed in a reduced space of Cartesian coordinates, following the method described in refs 4 and 21, which yields the lowest quasiadiabatic channel for the dissociation reaction in eq 3. These data have been inserted in the figure as marked points and were fitted with Morse potentials, shown as the upper, continuous curves in Figure 3a (with parameters $V_0/(hc) = 8018(8069)$ cm^{-1}, $\tilde{D} = 37852(37927)$ cm^{-1}, and $a = 1.885(1.871)$ $Å^{-1}$ for METPOT 3; values for METPOT 4 in parentheses).

The parameter α in the exponential decay model of eq 4 can be determined from the linear regression (shown in Figure 3b), which yields the values $\alpha = (0.80 \pm 0.03)$ $Å^{-1}$ for METPOT 3 and (0.66 ± 0.03) $Å^{-1}$ for METPOT 4. From the representation of the potentials in the logarithmic form, we see that there is a significant difference between the two parameter sets. We also observe that the data follow the linear exponential decay model only approximatively. Discrepancies from the linear behavior may arise from the DQMC analysis itself. Statistical and smaller systematic errors in the DQMC calculations can be as large as 50 cm^{-1}, in the range of Figure 3b. In the logarithmic scale of Figure 3b, these errors correspond to error bars in the size of the marks. However, in the limit $\Delta V(r) \rightarrow \Delta V(\infty)$, they become very large. Therefore only data up to $r(CH) = 3$ Å have been considered for the fit. On the other hand, a higher-order polynomial could be adjusted to the left-hand side of eq 4, which, in principle, is not excluded from the theoretical treatment in ref 22.

The value $\alpha \approx 1$ $Å^{-1}$ for the exponential interpolation parameter has frequently been assumed in previous work, where the rate constant for the thermal recombination reaction

$$(^2A''_2)CH_3 + (^2S_{1/2})H \rightarrow (^1A_1)CH_4 \qquad (8)$$

has been calculated within the statistical adiabatic channel model to be 4.5×10^{-10} cm^3 s^{-1} [23] (4.3×10^{-10} cm^3 s^{-1} (ref 38, $\alpha \approx 1$)). In ref 6, this assumption was tested within the two-dimensional model for the CH chromophore in CHD_3 with the result $\alpha \approx 0.84$ $Å^{-1}$. The recombination reaction in eq 8 has later also been analyzed with the potential surface of Duchovic, Hase, and Schlegel with different classical and semiclassical methods within different statistical theories.[39−43] The result of these calculations is a nearly temperature-independent rate constant 5×10^{-10} cm^3 s^{-1}. The experimental value is given by $(3.5 \pm 0.7) \times 10^{-10}$ cm^3 s^{-1} at 300 K.[44]

The procedure of using data from reaction kinetics to test the quality of potential surfaces may be questionable. First, statistical theories for the description of chemical reactions are based on the assumption that a microcanonical equilibrium distribution has been achieved in the reactant before the reaction occurs (after activation). This assumption cannot, in general, be justified a priori, which disables, to some extent, the use of statistical theories for testing the quality of potential surfaces.[45] Second, comparison with experiment is difficult because of the large, yet generally still accepted, differences between theoretical and experimental data in reaction kinetics. And third, restricting the representation of potential surfaces more or less to regions along a reaction path is possibly a limitation for the correct description of the reaction dynamics. In methane, the complicated global potential dependence on "nonreactive" coordinates is likely to be relevant for detailed quantum-dynamical calculations. In particular, the potential function along the CH bending coordinates ϑ and φ, as well as along the umbrella angle χ, is of great importance both for the dissociation reaction eq 3, as well as for the recombination in eq 8, and will be discussed below.

3.3. Potential along the CH Bending Angles. The question whether methane is able to perform a stereomutation reaction with a saddle point close to the dissociation threshold has been investigated previously (refs 46−48 and references therein). It has not yet been clarified to what extent the inversion motion of methane can influence the dissociation and recombination process. In Figure 4, the potential cut along the CH bond length is shown at different values of the CH bending angle ϑ, with $\varphi = 0°$ and planar CH_3 frame ($\chi = 90°$; see also Figure 1). The function shows the formation of a barrier for the recombination

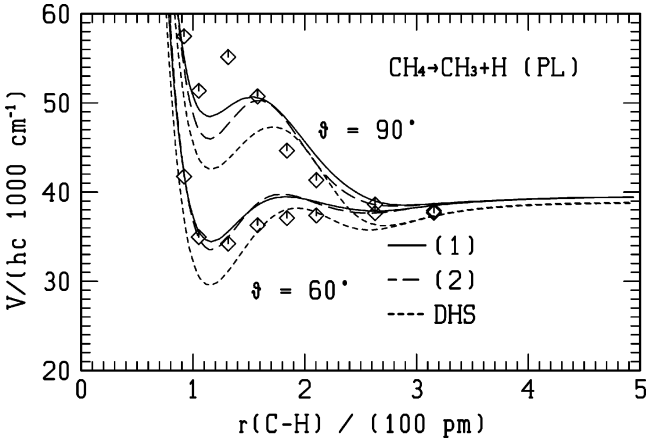

Figure 4. Lower curves: potential along r(CH) with planar CH_3 frame ($\chi = 90°$) and bent CH bond ($\vartheta = 60°$, $\varphi = 0°$). Upper curves: $\vartheta = 60°$, $\varphi = 0°$. Continuous curve (1) = METPOT 3, long-dashed curve (2) = METPOT 4, short-dashed curve DHS is from ref 8, and ◇ is from ref 36, 46 (ab initio MRD-CI).

reaction at the angle $\vartheta = 90°$. Barrier formation is possibly due to an avoided crossing of excited surfaces in the highly symmetric C_{2v} geometries for $\chi = \vartheta = 90°$, similar to the $NH_3 \rightarrow NH_2 + H$ dissociation in planar ammonia,[49] but this question is not further investigated here. At $\vartheta = 90°$, the ab initio values are roughly 5000 cm^{-1} higher than the results from the analytical representations of the present work and also show a more pronounced barrier, which becomes smaller for lower values of ϑ and which seems to disappear at $\vartheta = 60°$. The quantitative description of the ab initio data is nevertheless acceptable with discrepancies falling within the expected uncertainties of 2000−4000 cm^{-1} at energies above 0.8 aJ (~40 000 cm^{-1}), as given by eq 1 in paper I. The DHS surface[8] still shows a reasonable qualitative agreement with the ab initio data from the present work. We note that it was determined from the adjustment to the ab initio data set from ref 50, which was calculated at a slightly lower level than the data used here.[46]

The potential surface for the recombination reaction 8 can be analyzed in more detail in a two-dimensional cut. In $V(r,\chi)$ (shown in Figure 5), the CH bending angle ϑ is varied in a concerted way as a function of χ, such that $\vartheta(\chi = 109.47°) = 0°, \vartheta(\chi = 90°) = 90°, \vartheta(\chi = 180° - 109.47°) = 180°$. When all atoms are in a plane during the recombination ($\chi = \vartheta = 90°$), the stereoselection between the final states (potential minima) starts at very small bond lengths (roughly 2 Å), with rather low barriers for stereomutation. The height of these barriers will be discussed in detail in the next sections.

The potential along the bending angles ϑ and φ is shown in parts a and b of Figure 6. The CH bonds are kept at the equilibrium length (the CH_3 frame is pyramidal, $\chi = 109.47°$). Figure 6a corresponds to a cut at $\varphi = 0°$ ($\vartheta > 0$) and $\varphi = 180°$ ($\vartheta < 0$). The present analytical model potential gives, for the first time, a qualitatively correct description of a saddle point at $\vartheta = \chi = 109.47°$. Even the quantitative description of the ab initio data is acceptable within the error intervals from eq 1 in paper I. The data marked with an asterisk have not been used for the adjustment. At $\vartheta = -\chi$, two hydrogen atoms "collide", yielding very high energies which are not further described here. Clearly, the quartic force fields (GR[7] and LMT[9]) describe the bending potential only for bending angles falling in the range $|\vartheta| \lesssim 60°$.

The DHS potential from ref 8 does not describe the global bending potential correctly, even qualitatively. It is able to describe those parts of the potential surface, which are relevant for the CH bond rupture, neglecting regions with large displacements of bending coordinates. In Figure 6 of ref 41, a saddle point is shown at roughly 10 000 cm^{-1} below the dissociation threshold (repeated in ref 51, Figure 3.4), which is possibly a consequence of this neglect and disagrees with the present results from Figures 5 and 4.

The azimuthal potential shown in Figure 6b is entirely due to the H−H pair potential in eq 42 of paper I (because of condition eq 78 in that paper). The general behavior can be described even at very high energies, although the ab initio data above 2 aJ (100 000 cm^{-1} roughly) have not been used in the fits. The inclusion of excited electronic states, including ionization states, which are neglected in this work, would probably lead to significant changes of the ab initio data in these energy ranges. The nearly constant potential shape for energies below 0.35 aJ (~17 000 cm^{-1}) justifies, among other results, the success of the two-dimensional model of the CH chromophore potential for the description of the overtone spectrum in CHD_3 with nearly conservation of the quantum number l_b for the bending angular momentum.[30]

3.4. Methane Stereomutation. Inversion of methane becomes possible when the umbrella angle χ of the CH_3 frame is

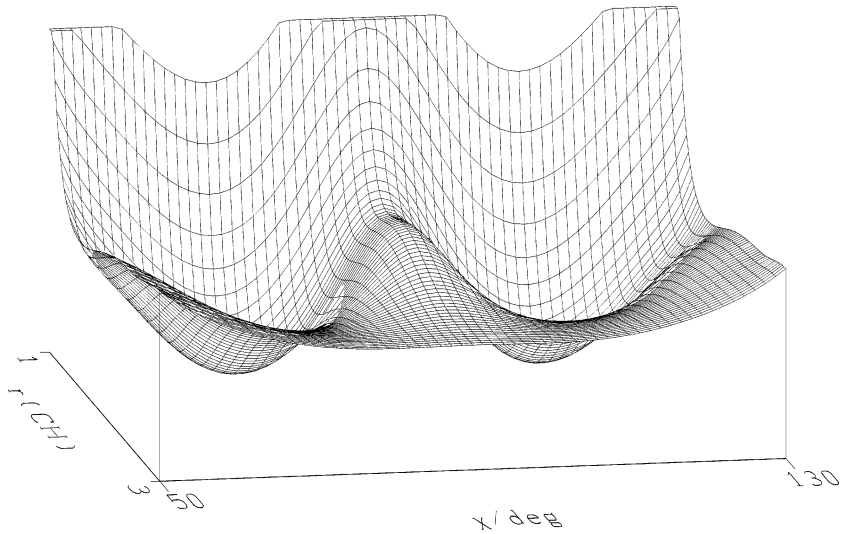

Figure 5. Potential along r(CH) and χ (see Figure 1). Front axis: χ (between 50° and 130°). The angle ϑ is varied according to $\vartheta = 4.6222(109.4712 - \chi)$. Rear axis: r(CH) (between 0.6 and 3 Å). Vertical axis: potential surface up to the equivalent of 100 000 cm^{-1}.

TABLE 1: Saddle Points for the CH_4 Stereomutation

	CH_4 (C_s)				CH_4 (C_{2v})		
	this work[a]	this work[b]	ref 48, Table 4	ref 47	this work[c]	ref 48, Scheme 1	ref 47
r_1/Å	1.196	1.167	1.300	1.316	1.278	1.170	1.194
r_2/Å	1.196	1.167	1.300	1.316	1.278	1.170	1.194
r_3/Å	1.069	1.078	1.134	1.131	1.057	1.070	1.079
r_4/Å	1.069	1.078	1.134	1.131	1.057	1.070	1.079
α_{12}	44.40°	54.25°	38.66°	37.54°	35.09°	43.65°	42.06°
α_{13}	78.30°	81.66°	76.57°	77.80°	89.82°	92.0°	92.5°
α_{14}	115.92°	127.52°	104.95°	105.90°	124.78°	135.67°	134.56°
α_{23}	115.92°	127.52°	104.95°	105.90°	124.78°	135.67°	134.56°
α_{24}	78.30°	81.66°	76.57°	77.80°	89.82°	92.0°	92.5°
α_{34}	116.20°	111.86°	95.64°	98.0°	145.28°	132.3°	133.0°
γ[d]	103.92°	117.80°	91.16°	92.90°	180.0°	180.0°	180.0°
E/aJ[e]	0.8127	0.7806	0.8571	0.8726	0.8848	0.8762	1.030

[a] METPOT 3. Harmonic wavenumbers (in cm^{-1}): 1732i, 410, 896, 1239, 1766, 1984, 2689, 3225, 3287 ("i" means an imaginary frequency). [b] METPOT 4. Harmonic wavenumbers (in cm^{-1}): 1771i, 586, 978, 1049, 1451, 2234, 2566, 3154, 3206. [c] METPOT 3. Harmonic wavenumbers (in cm^{-1}): 2091i, 1031i, 1313, 1475, 2014, 2362, 3252, 3427, 4168. [d] Angle between two CH_2 planes. [e] 1 aJ ≈ 50341 cm^{-1}.

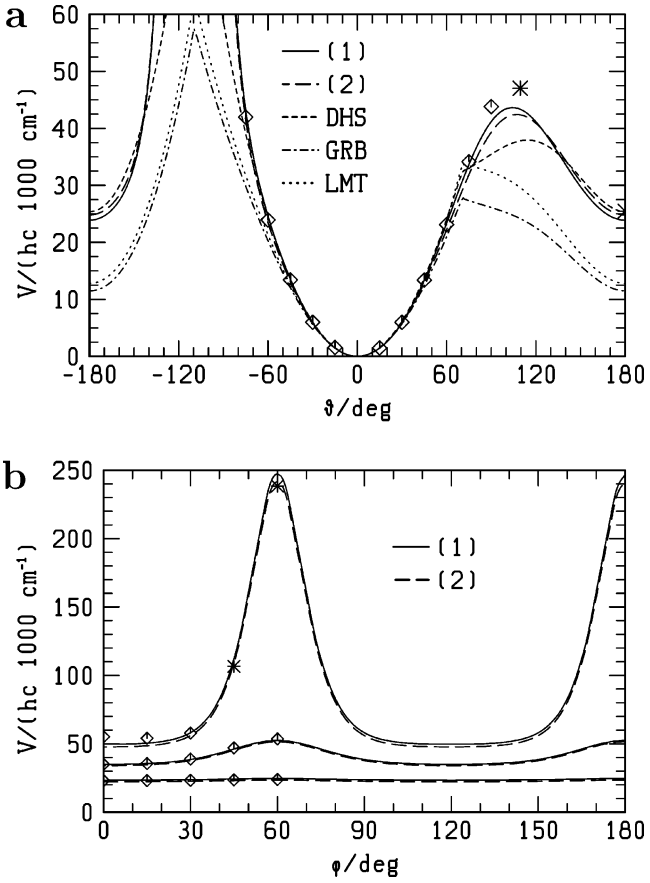

Figure 6. (a) Potential along ϑ at $r_i = r_e$ and $\chi = 109.47°$. (1) = METPOT 3, (2) = METPOT 4, DHS is from ref 8, GRB is from ref 7, LMT is from ref 9, ◇ and * are from ref 36 (* not fitted). (b) Potential along φ at $r_i = r_e$, $\vartheta = 60°$, 90°, $\chi = 109.47°$ (lower and uppermost curve), and $\vartheta = 60°$, $\chi = 90°$ (curve in the middle). ◇ and * are from ref 36 (* not fitted). (1) = METPOT 3, (2) = METPOT 4.

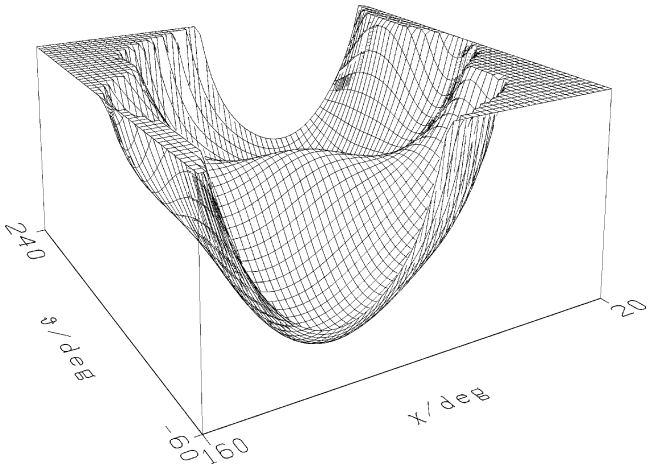

Figure 7. Perspective representation of the potential surface $V(\vartheta,\chi)$ (METPOT 3). Front axis: χ. Rear axis: ϑ. Vertical axis: potential surface up to the equivalent of 80 000 cm^{-1}.

also varied in Figure 6a. This is shown in Figure 7, where the two equivalent potential minima are located at the values $\vartheta = 0°$, $\chi = 109.47°$ (front) and $\vartheta = 180°$, $\chi = 70.53°$ (rear, behind the local maximum of roughly 50 000 cm^{-1} at $\vartheta = \chi = 90°$). The two equivalent saddle points are at approximately 42 000 cm^{-1}.

However, these are not true saddle points in the nine-dimensional space. A systematic search for stationary points in the complete space (using the algorithm described in ref 52) yields a saddle point with C_s structure at an energy of 0.814 aJ (~41 000 cm^{-1}) (for METPOT 3) with one imaginary frequency. A second point with C_{2v} structure was found at 0.885 aJ (~44 500 cm^{-1}) with two imaginary frequencies. The data are collected in Table 1, together with data from the literature,[47,48] for comparison, which were obtained from high-level, optimized ab initio calculations. The deviations characterize somewhat the expected uncertainty of the present model potential in the description of the true potential surface. The harmonic wavenumbers for the C_s saddle point given in Table 1 agree well with the data from ref 48.

Possible reaction paths for the stereomutation are shown in Figure 8. These are cuts along the corresponding paths of steepest descent (mass unweighted), which may start from the C_{2v} saddle (broken curve) or the C_s saddle point (continuous curve). The corresponding change of nuclear configurations are shown by snapshots for the C_{2v} (upper series) and C_s inversion motion (lower series).

3.5. Potential Surfaces for the H_2 Elimination and Abstraction Reactions. Further possible reactions occurring in the energy range of the simple CH bond rupture are the elimination of molecular hydrogen

$$(^1A_1)CH_4 \rightarrow (^3B_1)CH_2 + (^1\Sigma_g^+)H_2 \qquad (9)$$

with triplet methylene as product ($\Delta_R H_0^0 = 456$ kJ mol^{-1})[32] or

$$(^1A_1)CH_4 \rightarrow (^1A_1)CH_2 + (^1\Sigma_g^+)H_2 \qquad (10)$$

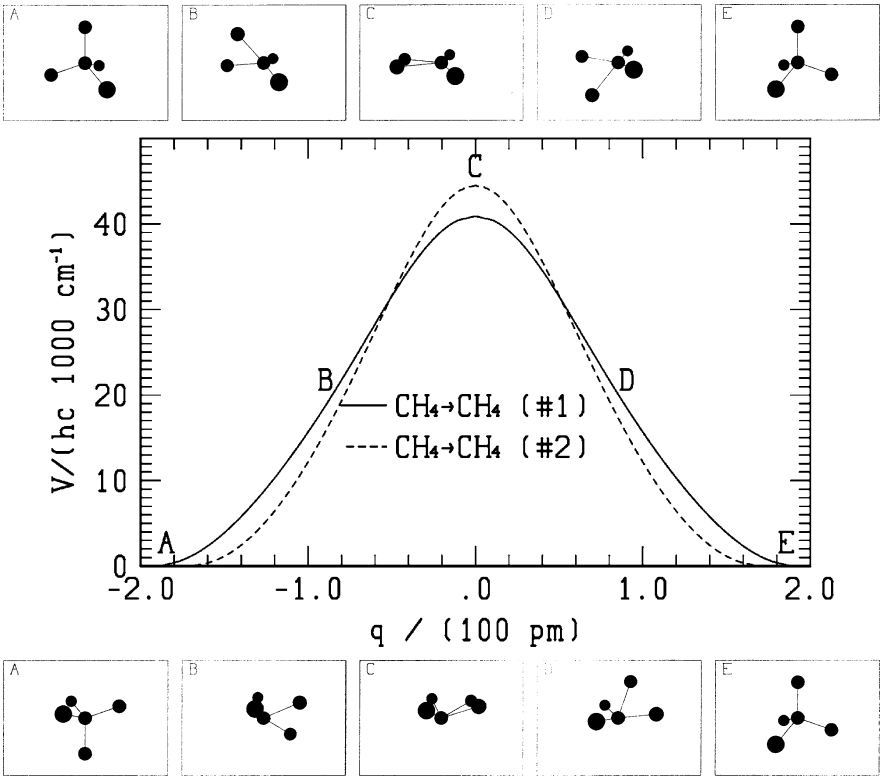

Figure 8. Potential and stereomutation motion of the nuclei over the C_{2v} saddle point (#2, broken curve, upper snapshot series) and the C_s saddle point (#1, continuous curve, lower series). The coordinate q follows the path of steepest descent.

with singlet methylene roughly 38 kJ mol^{-1} higher than for reaction eq 9.[53] Taking into account the zero-point energy within the harmonic approximation (with data from refs 31 and 54, see also Table 2 below), we obtain as expected reaction enthalpies on the electronic surface 0.899 aJ for singlet methylene (∼541 kJ mol^{-1}, 45 260 cm^{-1}) and 0.837 aJ for triplet methylene (∼503 kJ mol^{-1}, 42 110 cm^{-1}). In this work, we have considered the $(^3B_1)CH_2 + H_2$ reaction, which corresponds to an intersystem crossing. Such processes may be important in cases where the motion of the nuclei is very slow in regions where multivalued potential surfaces have intersections, so that couplings such as the spin−orbit coupling may be important.

The electronic energies in the triplet state are higher than in the singlet state for small values of the H_2-CH_2 distances. The surfaces cross at a distance between 1 and 2 Å (see Figure 9c; ★ marks triplet and ◇ marks singlet energies from the multireference determinant configuration interaction calculations, as described in paper I). The differences are, however, not very large. They induce the existence of a saddle point with C_{2v} structure for reaction eq 9 at 0.912 aJ (see also Figure 9d and Table 2 below).

The inverse reaction

$$(^3B_1)CH_2 + (^1\Sigma_g^+)H_2 \rightarrow (^1A_1)CH_4 \qquad (11)$$

corresponds to the insertion of molecular hydrogen into triplet methylene, for which we predict a barrier of 0.075 aJ (45 kJ mol^{-1}, 3800 cm^{-1}, with an uncertainty of at least 1500 cm^{-1}). Schaefer and co-workers have estimated the barrier for reaction 11 to be between 42 and 63 kJ mol^{-1}, while for the corresponding insertion into singlet methylene a Woodward−Hoffmann barrier of 113 kJ mol^{-1} is predicted, and the concerted, two-step insertion into singlet-methylene is expected to occur without barrier.[55] Figure 9d is very similar to Figure 3 of ref 56, in which the singlet diabatic version of the potential surface for the hydrogen elimination is shown.

For all practical purposes, the abstraction reaction

$$(^3B_1)CH_2 + (^1\Sigma_g^+)H_2 \rightarrow (^2A''_2)CH_3 + (^2S_{1/2})H \qquad (12)$$

is probably more important, since here the total spin is conserved. The barrier for this reaction is calculated to be 65 kJ mol^{-1}.[57] We find here a saddle point at 0.941 aJ for this reaction (see also Table 2 below), which yields a barrier of 0.104 aJ (63 kJ mol^{-1}) starting with $CH_2 + H_2$ (the geometry of the saddle point being similar to that from ref 57).

A summary of important stationary points in the present analytical representations of the global potential surface of methane is given in Table 2.

3.6. Zero-Point Energies, Equilibrium CH Bond Length. and Vibrationally Induced Electric Dipole Moment from DQMC Calculations. The DQMC algorithm is a very adequate tool, in connection with analytical representations of potential surfaces, to simulate the complete vibrational ground state structure of polyatomic molecules, and allows for an estimation of the anharmonic zero-point energy independently of perturbation theory.[4,58] In ref 5, we have developed a version of the DQMC method, commonly expressed in the Cartesian coordinates of the involved particles (see, for instance refs 4 and 59), in which the Hamiltonian is first formulated in the normal coordinates as derived by Watson.[29] We then used harmonic wave functions as test functions, by means of which the statistical fluctuations in the simulation could be kept significantly small. A small systematic error due to the neglect of vibrational angular momentum parts in Watson's Hamiltonian (Coriolis interaction) has also been estimated.

Results for the zero-point energy of several isotopomers obtained from DQMC calculations are collected in the two last columns of Table 3. Estimated contributions from the Coriolis interaction and pseudopotential are included. The values may be compared with the zero-point energy in the harmonic

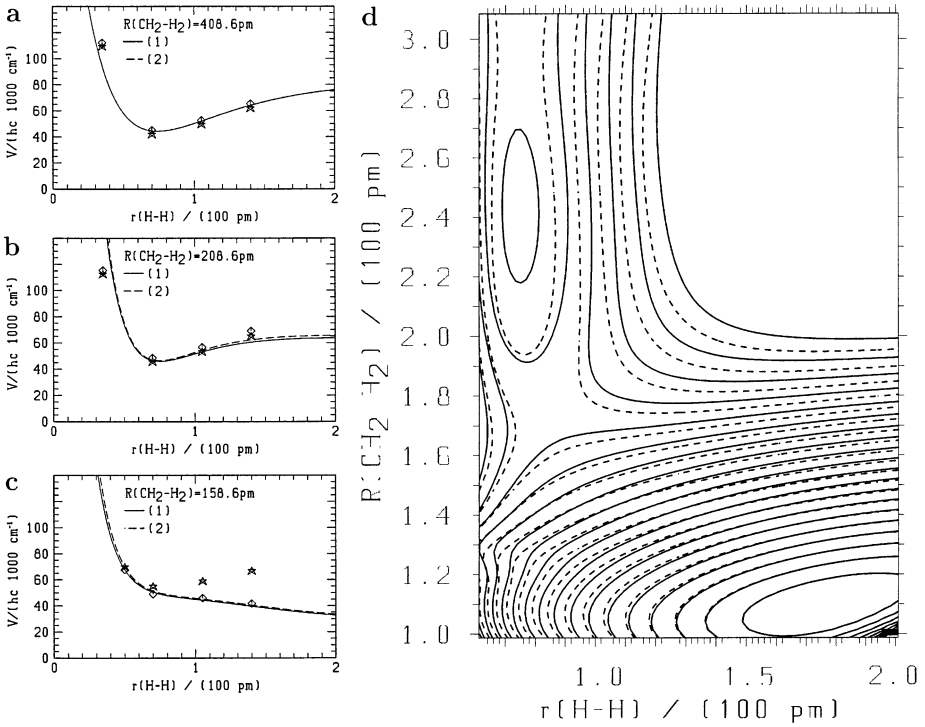

Figure 9. Potential cuts along r_{12} (the distance between hydrogen atoms 1 and 2, r(H−H)) at different values of $r_1 = r_2 = R$ (for this purpose, the structure in Figure 1 is varied along ϑ, r_1, and r_2). (a) $R = 4.086$ Å. ★ are triplet energies and ◇ are singlet energies from MRD-CI calculations (see paper I). (1) = METPOT 3, (2) = METPOT 4. (b) $R = 2.086$ Å. (c) $R = 1.586$ Å. (d) Contour plot of the potential along r_{12} and $r_1 = r_2 = R$. Equidistant potential curves (lowest value at 3000, highest value at 60 000, distance between the level curves 3000 cm^{-1}). For the elimination reaction eq 9, there is at least one saddle point given by the coordinates $r_1 = r_2 = 1.83$ Å, $r_3 = r_4 = 1.085$ Å, $\alpha_{12} = 25.14°$, $\alpha_{13} = \alpha_{14} = \alpha_{23} = \alpha_{24} = 108.55°$ and $\alpha_{34} = 141.86°$. There is a shallow local minimum in the figure, located behind the barrier (at roughly 40 000 cm^{-1}). Continuous level curves = METPOT 3, broken level curves = METPOT 4.

approximation, shown in the first column and including anharmonic effects obtained from perturbation theory by calculation of the quartic force field in normal coordinates and spectroscopic constants (cf. ref 60, page 160)

$$E_{zp}/hc = \frac{1}{2}\sum_k \omega_k d_k + \frac{1}{4}\sum_{k\geq l} x_{kl} d_k d_l. \qquad (13)$$

In general, the DQMC results lie between the harmonic and anharmonic estimations. Contributions from anharmonic resonances are not included in the anharmonic constants x_{kl} of eq 13. The potential from ref 7 was used as a test of our procedure The results for the x_{kl} are similar to the values obtained in ref 7, Table 8 for nearly all isotopomers of methane, the corresponding anharmonic zero-point energy estimation is also given in Table 3. The zero-point energy for CH_4 corresponds to 9691.53 cm^{-1} in ref 16 from a full-dimensional variational calculation on another recently developed potential-energy surface,[12] which is above the values obtained here from perturbation theory but below the values from the DQMC calculations.

Grev, Janssen, and Schaefer[61] have discussed the possible error of zero-point energy estimations from calculated fundamental transitions ($^1/_2\sum_i \tilde{\nu}_i$), compared to the anharmonic zero-point energy from eq 13. Specifically for CH_4, the error of SCF calculations, scaled to reproduce experimental fundamentals, was calculated to be 0.94 kcal mol^{-1} (∼3.9 kJ mol^{-1}).[61] These authors suggested a better estimation of the zero-point energy by considering the average $^1/_4\sum_i(\tilde{\nu}_i + \omega_i)$. However, the latter is generally still *lower* than the value from eq 13 (see also ref 61), which has been shown in Table 3 to be lower than the more certain estimation from the DQMC calculation by roughly 0.8 kJ mol^{-1}, in the worst case (for CH_3). We conclude that, even following the procedure suggested in ref 61, the error in the estimation of the anharmonic zero-point energy from perturbation theory may be as large as 1 kJ mol^{-1}, for strongly covalent bonded molecules such as methane. The error can be larger for floppy molecules, or when strong anharmonic resonances are neglected.

DQMC calculations have also been used, in our previous work,[5] to discuss the role of ab initio calculations of the equilibrium CH bond length in methane, which have received great attention in the past (see, for instance, refs 6, 9, 62−65), in comparison with experimental results. Obviously, the true value of r_e should be compatible with experimental values, e.g., for rotational constants, under inclusion of the vibrational structure at equilibrium. In this sense, we have also tested the validity of perturbation theory, normally used for the determination of B_e values from experimentally accessible rotational constants B_v for all isotopomers. We calculated B_0 values in the vibrational ground state by solving the Schrödinger equation in the complete space of internal vibrations with the DQMC algorithm and the analytical potential representation METPOT 1.[5] From the comparison of the results with the experimental values, we concluded that the equilibrium CH bond length is $r_e = (1.086 \pm 0.002)$ Å, confirming former estimations.[6,7] We have repeated the calculations subsequently with the more recent model potentials METPOT 2−METPOT 4 and obtained the same result for r_e. Results for the averaged rotational constants $\langle B_0 \rangle$ calculated with METPOT 3 are collected in Table 4.

Similarly, we have calculated the vibrationally induced electric dipole moment of the methane isotopomers CH_3D, CH_2D_2, and CHD_3 by modeling the electric dipole-moment vector operator with an analytical representation to describe the intensity distribution in the overtone spectrum of CHD_3 (see also Table 9 below) and using the potential surface representa-

TABLE 2: Summary of Stationary Points on the Analytical Potential Surfaces of Methane (CH_4): Geometries, Energies, and Second Derivatives

	model METPOT	r_i/Å α_{ij}/(deg)	E/hc cm^{-1}	E_{zp}/hc cm^{-1}	$(\partial^2 E/(\partial Q_j^2))^{1/2}/2\pi c$ cm^{-1} [a]									
T_d	3 + 4	1.086 (4) 109.47 (6)	0	9730[b]	3157	3157	3157	3025	1582	1582	1367	1367	1367	
D_{3h}[d]	3 + 4	1.079 (3) 120.00 (3)	39500	6441[b]	3276	3276	3199	1412	1412	520				
C_{2v}[e]	3 + 4	1.075 (2) 134.00	41860	3687[c]	3217	3071	1084							
		H_2: $r_{HH} = 0.741$	$D_e = 38289$	2202[c]	4404									
C_s (#1)[f]	3	1.196 1.196 1.069 1.069 44.4 78.3 115.9 115.9 78.3 116.2	40912	7748[c]	3287	3225	2689	1984	1766	1239	896	410	1732*i*	
	4	1.167 1.167 1.078 1.078 54.3 81.7 127.5 127.5 81.7 111.9	39294	8497[c]	3206	3154	2566	2234	1451	1049	978	586	1771*i*	
C_{2v} (#2)[f]	3	1.278 1.278 1.057 1.057 35.1 89.8 124.8 124.8 89.8 145.3	44542	9006[c]	4168	3427	3252	2362	2014	1475	1313	1031*i*	2091*i*	
	4	1.160 1.160 1.066 1.066 57.9 89.9 147.7 147.7 89.9 122.2	41511	8995[c]	3347	3279	2633	2227	1657	841	8073	857*i*	2144*i*	
C_{2v} (#3)[g]	3	1.830 1.830 1.085 1.085 25.1 108.6 108.6 108.6 108.6 141.9	45900	7464[c]	3749	3248	3044	1396	1190	971	916	413	1419*i*	
	4	1.776 1.776 1.079 1.079 26.6 108.5 108.5 108.5 108.5 141.9	46870	8152[c]	3459	3341	3125	1478	1332	1023	665	239	1642*i*	
C_{2v} (#4)[h]	3	2.414 1.560 1.082 1.082 0.0 113.9 113.9 113.9 113.9 132.3	47356	6006[c]	3251	3094	2256	1256	1169	499	487	167*i*	2126*i*	
	4	2.393 1.541 1.081 1.081 0.0 113.9 113.9 113.9 113.9 132.3	46400	7528[c]	3292	3153	2350	1357	1318	665	543	288	2110*i*	

[a] Normal coordinates relative to the stationary point, negative second derivative lead to imaginary frequencies, isotopic masses $m(H) = 1.00725$ u, $m(C) = 12.0$ u. [b] Anharmonic zero-point energy from DQMC for METPOT 3 only. [c] Harmonic zero-point energy as sum over real frequencies (separately for two fragments). [d] $CH_3 + H$. [e] $(^3B_1)CH_2 + H_2$. [f] Stereomutation. [g] $CH_4 \rightarrow (^3B_1)CH_2 + H_2$. [h] $H + CH_3 \rightarrow (^3B_1)CH_2 + H_2$.

TABLE 3: Methane Zero-Point Energies E_{zp}/hc in cm^{-1}

		anharmonic (perturbation theory)[b]			anharmonic (DQMC)[c]	
isotope[a]	harmonic	METPOT 3	METPOT 4	ref 7	METPOT 3	METPOT 4
CH_4	9880	9676	9672	9661	9730	9716
CH_3D	9237	9118	9081	9091	9106	9087
CH_2D_2	8583	8444	8437	8428	8464	8457
CHD_3	7919	7818	7803	7805	7819	7810
CD_4	7245	7133	7132	7145	7160	7154
CH_3	6548	6372	6376		6441	6449

[a] Isotopic masses as in Table 4. [b] From eq 13 with anharmonic constants from an analysis of the quartic force field, cf. Table 5. [c] DQMC; values including correction for Coriolis interaction (cf. ref 5, eq 5); the statistical error is roughly 2 cm^{-1} (95% confidence interval) for all values. [d] METPOT 3. [e] METPOT 4. [f] Reference 7.

tions METPOT 1[5] and METPOT 2.[11] Here, we repeated the calculations with the model METPOT 3, using the nine-dimensional dipole-moment function in eq 1 and obtained the results $(6.3 \pm 0.5) \times 10^{-3}$ (CH_3D), $(7.1 \pm 0.5) \times 10^{-3}$ (CH_2D_2), and $(6.4 \pm 0.4) \times 10^{-3}$ Debye (CHD_3) for μ_0, consistent with our previous results (for the definition of axes and signs see Figure 1 in ref 11; error bars refer to a 95% confidence interval from the DQMC calculations).

3.7. Quartic Force Fields. To compare the present analytical representation directly with other potential surfaces of methane, generally given as polynomial expansions around the equilibrium structure, we have calculated, in Table 5, the quartic force field in T_d symmetry coordinates.[7,9,66] The values were obtained numerically with a method of finite differences, in which each partial derivative of order j was calculated with a differentiation formula with $j + 1$ pivots at distances of typically $\Delta r = 10^{-4}$ Å.

The potential models from refs 7 (GR) and 9 (LMT) have been evaluated with the same numerical method here, which yields force fields identical with those from the literature. Up to cubic order, all force fields in Table 5 are rather similar. In the quartic order, larger discrepancies are apparent. The GR and LMT potentials are true polynomial forms, with parameters obtained by adjustment to data to determine the potential surface in the vicinity of the equilibrium structure. These are either spectra in the fundamental region (GR), or CCSD(T) energies (LMT). We may say, that these potentials have been determined to give an optimal description of the potential surface close to equilibrium. However, it may be asked whether these values would not change significantly if contributions from quintic or higher orders were included.[10]

The potential models from the present work and DHS[8] are, on the other hand, global forms, in which the force constants from Table 5 correspond to lowest-order contributions of large (in principle infinite) Taylor expansions of the potential surface. These forms have not been especially optimized to represent the potential surface in the neighborhood of the equilibrium. Of further interest for the comparison between different force fields is a comparison of fundamental transitions, calculated most easily within the perturbation theory for asymmetric tops in ref 60 (page 160). In Table 6, we compare the fundamental transitions in CH_2D_2. The results from the polynomial forms are certainly in better agreement with the experimental data. However, except for ν_2, the results from the global forms deviate not more than 30 cm^{-1} from the experimental data (additionally, these forms have different harmonic force fields). For METPOT 4 (last column), which corresponds to an experimentally refined anharmonic force field with respect to the overtone spectrum

TABLE 4: Averaged Rotational Constants $\langle B_0 \rangle$ (in cm^{-1}) in the Vibrational Ground State of Several Methane Isotopomers[a]

	exp	ref	DQMC[b]
CH_4	5.24104633	89	5.248 ± 0.012
CH_3D	4.33707	90	4.339 ± 0.012
CH_2D_2	3.61964	91	3.624 ± 0.011
CHD_3	3.06243	92	3.065 ± 0.011
CD_4	2.632729	93	2.636 ± 0.008

[a] $\langle B_0 \rangle \equiv (A_0 + B_0 + C_0)/3$; isotopic masses $m_H = 1.007825$ u, $m_D = 2.014$ u, $m_C = 12$ u. [b] Results from the complete solution of the Schrödinger equation on the analytical potential surface METPOT 3 with DQMC in a normal coordinate space (cf. ref 5). Error bars give the 95% confidence interval (corrections for Coriolis interaction terms included).

of CHD_3 (to be discussed below), the deviations are between 10 and 20 cm^{-1}, except for ν_2.

The assumption that perturbation theory is a good approximation is not necessarily valid. For CH_2D_2 for instance, ν_2 and ν_8 are coupled by a Fermi resonance to $2\nu_7$ and $\nu_4 + \nu_9$, respectively, and contributions from force fields of higher orders may significantly shift these numbers when (exact) variational calculations are performed. This point will be discussed in detail in the next section.

3.8. The Overtone Spectrum in CHD_3. The vibrational (rotational) spectrum of CHD_3 in the mid and near infrared is dominated by a regular series of band groups (polyads), which can essentially be assigned to the group vibrations of the CH chromophore.[6,46,67−77] Experimental band positions are given in the first column of Table 7. A detailed analysis of the spectra, generally recorded under high-resolution conditions, may be found in the literature. The general structure of this polyad series is characteristic for the overtone spectrum of compounds of the type CHX_3 (also of asymmetric tops CHXYZ) and is related to a "universal" Fermi resonance between the stretching and bending manifolds of this group[25] (see also refs 76, 78, 79). This structure has been described by two- and three-dimensional potential models, such as the model in normal coordinates from Lewerenz and Quack (V_{CH}^{LQ}, see eq 5). Figure 10 shows two possible representations following METPOT 3 and METPOT 4 (2-dimensional cuts).

In column "I" of Table 7, we first give the theoretical line positions from a new fit of V_{CH}^{LQ} to the experimental line positions (all data from column "$\tilde{\nu}_{obs}$", including data above 17 000 cm^{-1}). In this fit, the conversion from the polar to the normal coordinates representation was performed on a larger grid than in ref 6, and the surface energies have been weighted with the weight function

$$w(E) = \exp(-\ln(2)(E/E_{half})^2) \qquad (14)$$

All relevant parameter values are given in Table 8, the new adjusted parameter values in column "I" (for comparison, previously used parameter values are given in column "0"). In ref 6, the model was fitted to band positions up to 17 000 cm^{-1} only. However, the agreement of line positions with experimental data above 17 000 cm^{-1}, with uncertain assignment[70] or measured later with greater precision,[72,73] was already rather good there. In Table 8, we give the leading coefficients of the Taylor expansion in Cartesian normal coordinates. We note that these coefficients do not contain the complete information to calculate the spectrum.[6] We also give the constants of the effective Hamiltonian (cf. eqs 3 and 4 in ref 6). The effective Fermi resonance coupling constant from a fit to the theoretical spectrum from the variational calculation is $k'_{sbb} \approx 15$ cm^{-1}.

TABLE 5: Quartic Force Field of Methane in the Electronic Ground State[a]

	this work[b]	LMT[9]	GRB[7]	DHS[8]
r^{eq}/Å	1.08580	1.08900	1.08580	1.08600
F_{11}/aJ Å^{-2}	5.43512	5.46863	5.43498	5.46273
F_{22}/aJ	0.58401	0.57919	0.58400	0.59380
F_{33}/aJ Å^{-2}	5.37813	5.36600	5.37798	5.53692
F_{34}/aJ Å^{-1}	−0.22100	−0.21036	−0.22100	−0.25750
F_{44}/aJ	0.54801	0.53227	0.54800	0.59380
F_{111}/aJ Å^{-3}	−14.69890	−15.17108	−15.29994	−15.48866
$F_{12_a2_a}$/aJ Å^{-1}	−0.10328	−0.25438	−0.29900	−0.22860
$F_{13_x3_x}$/aJ Å^{-3}	−14.51342	−15.49766	−15.68994	−15.25525
$F_{13_x4_x}$/aJ Å^{-2}	0.10419	0.06598	0.06600	−0.05148
$F_{14_x4_x}$/aJ Å^{-1}	−0.38421	−0.22556	−0.11000	−0.13279
$F_{2_a2_a2_a2_a}$/aJ	0.33916	0.09116	0.09400	0.10248
$F_{2_a3_z3_z}$/aJ Å^{-2}	−0.20445	−0.35605	−0.37000	−0.04340
$F_{2_a3_z4_z}$/aJ Å^{-1}	0.25462	0.18004	0.16000	0.14088
$F_{2_a4_z4_z}$/aJ	−0.41442	−0.34330	−0.31100	−0.31281
$F_{3_x3_y3_z}$/aJ Å^{-3}	−14.46115	−15.57540	−15.86993	−15.14125
$F_{3_x3_y4_z}$/aJ Å^{-2}	−0.02049	−0.21811	−0.26800	−0.26627
$F_{3_x4_y4_z}$/aJ Å^{-1}	−0.06227	−0.09616	−0.10100	−0.11514
$F_{4_x4_y4_z}$/aJ	0.27299	0.34391	0.34500	0.31707
F_{1111}/aJ Å^{-4}	30.09040	37.40723	43.24017	34.68589
$F_{112_a2_a}$/aJ Å^{-2}	−0.53367	−0.01264	0.00000	−0.20810
$F_{113_x3_x}$/aJ Å^{-4}	31.42069	39.79558	43.24022	34.70211
$F_{113_x4_x}$/aJ Å^{-3}	−1.67468	0.21867	−0.00020	0.61229
$F_{114_x4_x}$/aJ Å^{-2}	0.20361	0.05929	0.00000	−0.16831
$F_{12_a2_a2_a}$/aJ Å^{-1}	−1.25762	−0.06147	0.00000	−0.17727
$F_{12_a3_z3_z}$/aJ Å^{-3}	−2.80482	0.06888	0.00000	−0.11666
$F_{12_a3_z4_z}$/aJ Å^{-2}	−0.16518	−0.04273	0.00000	0.18290
$F_{12_a4_z4_z}$/aJ Å^{-1}	−2.70612	0.14474	0.00000	0.02300
$F_{13_x3_y3_z}$/aJ Å^{-4}	36.05075	40.63881	43.24024	34.77557
$F_{13_x3_y4_z}$/aJ Å^{-3}	−1.66491	0.11840	−0.00020	0.34192
$F_{13_x4_y4_z}$/aJ Å^{-2}	0.00750	−0.02093	0.00000	−0.00744
$F_{14_x4_y4_z}$/aJ Å^{-1}	−0.35288	−0.16567	0.00000	−0.12185
$F_{2_a2_a2_a2_a2_a}$/aJ	1.52545	0.17338	0.00030	−0.24067
$F_{2_a2_a3_z3_z}$/aJ Å^{-2}	0.34967	−0.19706	0.00000	−0.10562
$F_{2_b2_b3_z3_z}$/aJ Å^{-2}	0.86673	−0.43249	0.00000	−0.24861
$F_{2_a2_a3_z4_z}$/aJ Å^{-1}	−1.78526	−0.13777	0.00000	−0.11953
$F_{2_b2_b3_z4_z}$/aJ Å^{-1}	−1.17561	−0.04896	−0.00014	0.03044
$F_{2_a2_a4_z4_z}$/aJ	0.96280	0.01740	−0.00004	0.20194
$F_{2_b2_b4_z4_z}$/aJ	0.40702	0.37668	0.00000	0.10601
$F_{2_a3_x3_y4_z}$/aJ Å^{-2}	−0.88891	0.27554	0.00000	0.19315
$F_{2_a3_z4_x4_y}$/aJ Å^{-1}	0.00610	−0.06801	0.00000	−0.01100
$F_{3_x3_y3_z3_z}$/aJ Å^{-4}	31.82206	41.03733	43.24027	34.58544
$F_{3_x3_x3_y3_y}$/aJ Å^{-4}	32.95466	41.13063	43.24027	34.83520
$F_{3_x3_x3_y4_x}$/aJ Å^{-3}	−3.12347	0.18466	−0.00020	0.35304
$F_{3_x3_x3_y4_y}$/aJ Å^{-3}	−1.84453	0.32592	−0.00020	0.44937
$F_{3_x3_y4_x4_x}$/aJ Å^{-2}	1.58276	0.09940	0.00000	−0.00169
$F_{3_x3_y4_x4_y}$/aJ Å^{-2}	0.26689	−0.00523	0.00000	−0.08113
$F_{3_x3_x4_y4_y}$/aJ Å^{-2}	0.91924	−0.24415	0.00000	−0.22561
$F_{3_x4_x4_x4_x}$/aJ Å^{-1}	−3.51801	−0.39593	−0.00007	−0.35331
$F_{3_x4_x4_y4_y}$/aJ Å^{-1}	−2.28680	−0.14836	−0.00014	−0.05273
$F_{4_x4_x4_x4_x}$/aJ	4.04675	0.49842	−0.00034	1.05230
$F_{4_x4_x4_y4_y}$/aJ	5.99584	0.70977	0.00000	0.30289

[a] Force field in T_d symmetry (cf. refs 7, 9, and 66); 1 Å = 100 pm. [b] METPOT 3

TABLE 6: Fundamental Transitions in CH_2D_2 (in cm^{-1})

	exp	GRB[7]	LMT[9]	DHS[8] [a]	this work[b]	this work[c]
ν_1 (A_1)	2975.5[94]	2977.1	2972.1	2991.9	2958.8	2965.7
ν_2 (A_1)	2203.2[7]	2134.8	2241.5	2170.9	2146.1	2143.6
ν_3 (A_1)	1435.1[95]	1435.9	1435.7	1472.9	1460.3	1439.0
ν_4 (A_1)	1033.1[95]	1033.3	1033.9	1076.7	1050.7	1040.9
ν_5 (A_2)	1331.4[95]	1331.9	1330.8	1347.1	1362.0	1332.8
ν_6 (B_1)	3012.3[7]	3012.8	3008.0	3039.5	3003.0	3009.1
ν_7 (B_1)	1091.2[95]	1092.6	1093.5	1153.6	1101.6	1105.9
ν_8 (B_2)	2235.7[91]	2217.7	2232.3	2262.5	2233.2	2232.5
ν_9 (B_2)	1236.3[95]	1235.7	1238.6	1308.6	1249.1	1254.4

[a] Calculated without the contributions from eqs 27 and 28 in ref 8. [b] METPOT 3. [c] METPOT 4.

This value cannot be determined from the spectrum of CHD_3 with much certainty, because the averaged deviation of the fit

TABLE 7: Wavenumbers of the Overtone Spectrum of the CH Chromophore in CHD_3 (in cm^{-1})

		$\tilde{\nu}_{the}$[b]						
N_j[a]	$\tilde{\nu}_{obs}$[a]	I	II	III	IV	V	VI	VII
$(1/2)_1$	1292.50[74]	1291.61	1317.79	1309.60	1313.29	1306.10	1335.84	1299.87
1_2	2564.67[6]	2567.90	2622.60	2598.56	2612.52	2590.61	2646.93	2580.26
1_1	2992.75[6]	2990.81	2980.75	2986.67	2985.04	2987.41	3018.98	3058.05
$(3/2)_2$		3840.00	3928.88	3885.13	3910.71	3874.66	3956.30	3856.84
$(3/2)_1$	4262.10[6]	4259.99	4271.94	4270.70	4270.40	4267.84	4331.63	4344.83
2_3		5097.41	5220.83	5151.30	5194.52	5137.34	5241.27	5114.64
2_2	5515.70[6]	5515.35	5550.02	5533.74	5542.08	5525.69	5617.53	5612.68
2_1	5864.98[6]	5865.90	5842.02	5858.30	5855.49	5859.86	5916.96	6059.59
$(5/2)_3$		6351.42	6513.08	6415.24	6476.99	6399.53	6524.68	6369.24
$(5/2)_2$		6766.89	6829.76	6794.36	6812.81	6782.96	6901.70	6876.72
$(5/2)_1$	7115.48[6]	7112.67	7108.02	7117.56	7113.42	7115.44	7208.35	7333.41
3_4		7591.44	7788.97	7658.86	7744.39	7640.27	7783.84	7605.87
3_3	8005.40[6]	8004.76	8094.51	8034.07	8069.27	8017.96	8159.57	8122.31
3_2	8347.106	8347.01	8360.71	8354.98	8358.06	8346.94	8468.76	8588.67
3_1	8623.32[6]	8625.50	8585.04	8615.66	8611.82	8618.15	8696.27	9004.64
$(7/2)_4$		8828.78	9063.62	8900.31	9009.88	8880.42	9041.58	8839.91
$(7/2)_3$		9239.36	9359.18	9271.37	9324.29	9252.16	9415.76	9364.68
$(7/2)_2$		9577.98	9615.43	9590.02	9602.02	9577.86	9727.93	9840.16
$(7/2)_1$	9852.76[6]	9850.23	9829.16	9851.83	9843.46	9850.58	9970.33	10265.60
4_5		10052.70	10319.59	10121.55	10259.31	10099.21	10275.49	10056.76
4_4		10460.59	10605.70	10487.63	10563.90	10463.74	10645.66	10589.33
4_3		10796.07	10853.39	10803.00	10831.58	10784.98	10957.12	11073.42
4_2	11063.60[6]	11063.74	11058.60	11063.89	11062.19	11056.01	11201.96	11508.23
4_1	11268.80[6]	11270.14	11213.46	11260.60	11255.03	11264.17	11363.90	11893.20
$(9/2)_5$		11274.41	11572.85	11340.85	11506.07	11317.78	11508.71	11271.64
$(9/2)_4$		11679.12	11849.88	11701.46	11801.15	11674.25	11873.95	11811.38
$(9/2)_3$		12011.02	12090.39	12013.45	12059.54	11990.99	12184.98	12303.43
$(9/2)_2$		12274.45	12290.27	12273.85	12280.68	12261.18	12436.34	12747.09
$(9/2)_1$	12476.127[3]	12474.05	12444.30	12477.22	12463.16	12477.00	12628.15	13141.42
5_6		12483.01	12805.64	12540.67	12735.80	12516.29	12719.97	12470.13
5_5		12884.47	13072.47	12894.24	13021.44	12862.16	13076.35	13016.48
5_4		13212.77	13305.24	13201.34	13271.02	13172.44	13382.70	13515.92
5_3		13472.45	13499.26	13459.09	13483.78	13439.52	13631.84	13967.85
5_2	13664.68[75]	13667.44	13647.85	13662.52	13657.93	13655.04	13812.57	14371.32
$(11/2)_6$		13689.82	14035.20	13739.87	13962.45	13716.59	13933.24	13667.32
5_1	13799.35[75]	13801.50	13744.03	13798.75	13788.20	13803.38	13944.13	14725.28
$(11/2)_5$		14087.42	14290.71	14084.92	14238.25	14049.41	14277.93	14219.61
$(11/2)_4$		14411.57	14516.03	14386.49	14479.29	14352.29	14579.06	14725.82
$(11/2)_3$		14667.19	14705.89	14641.85	14684.68	14616.62	14829.47	15185.36
$(11/2)_2$	14856.82[73]	14858.37	14857.53	14847.71	14852.79	14835.08	15028.54	15597.48
6_7		14884.08	15244.46	14922.51	15172.14	14901.21	15129.95	14849.04
$(11/2)_1$	14990.69[73]	14988.76	14984.27	15003.57	14980.42	15003.92	15206.05	15960.84
6_6		15277.10	15484.50	15255.53	15436.56	15215.57	15455.60	15406.57
6_5		15596.54	15699.43	15548.74	15668.29	15507.32	15745.25	15918.96
6_4		15847.49	15880.83	15798.70	15865.92	15765.51	15987.76	16385.46
6_3		16034.23	16019.80	16001.06	16027.55	15980.93	16170.06	16805.53
$(13/2)_7$		16077.71	16451.68	16108.20	16379.82	16092.09	16334.09	16030.32
6_2	16156.91[72]	16160.22	16122.39	16147.79	16149.17	16142.14	16307.82	17177.92
6_1	16230.67[77]	16229.51	16249.89	16252.53	16226.82	16255.58	16481.30	17500.87
$(13/2)_6$		16464.48	16672.75	16425.53	16630.55	16382.96	16634.95	16592.22
$(13/2)_5$		16778.15	16876.57	16708.39	16852.10	16661.01	16910.68	17110.12
$(13/2)_4$		17023.68	17052.01	16952.62	17042.12	16912.60	17148.48	17582.99
$(13/2)_3$		17205.40	17198.20	17154.03	17198.63	17127.51	17344.07	18010.34
7_8		17261.07	17640.72	17283.61	17573.22	17274.73	17530.15	17197.53
$(13/2)_2$		17329.05	17340.12	17313.39	17321.35	17301.62	17526.10	18391.27
$(13/2)_1$		17417.52	17507.35	17456.18	17425.52	17453.72	17734.17	18723.87
7_7		17638.86	17835.09	17578.49	17805.34	17533.40	17795.11	17763.01
7_6		17944.79	18021.42	17845.37	18013.58	17790.80	18046.67	18285.53
7_5		18182.70	18181.14	18078.99	18193.37	18030.24	18267.40	18763.98
7_4		18355.46	18300.73	18272.08	18340.61	18237.38	18436.02	19197.82
$(15/2)_8$		18446.90	18827.22	18467.38	18767.62	18468.11	18738.61	18365.47
7_3	18465.56[72]	18463.32	18418.17	18414.92	18449.14	18398.44	18576.00	19586.42
7_2	18531.23[72]	18530.71	18576.52	18526.40	18532.98	18519.38	18759.60	19928.02
7_1		18625.04	18770.41	18670.58	18643.94	18665.14	18986.49	20219.96
$(15/2)_7$		18811.09	18991.96	18734.18	18975.73	18688.56	18960.80	18933.35
$(15/2)_6$		19106.49	19159.82	18980.91	19167.88	18920.75	19183.87	19459.65
$(15/2)_5$		19334.93	19311.99	19202.37	19336.78	19146.48	19391.18	19943.06
$(15/2)_4$		19497.31	19454.02	19390.28	19477.20	19348.50	19572.66	20382.80
$(15/2)_3$		19603.75	19614.75	19544.95	19593.84	19519.39	19756.78	20778.38
8_9		19629.68	19991.05	19647.09	19952.38	19659.13	19944.98	19525.35
$(15/2)_2$		19704.29	19806.40	19694.82	19713.89	19678.30	19972.98	21128.51
$(15/2)_1$		19830.01	20029.12	19868.73	19857.64	19856.93	20224.00	21430.50

TABLE 7 (Continued)

		$\tilde{\nu}_{the}$[b]						
N_j[a]	$\tilde{\nu}_{obs}$[a]	I	II	III	IV	V	VI	VII
8_8		19979.23	20121.98	19874.49	20127.16	19829.55	20110.56	20099.20
8_7		20262.46	20261.11	20088.03	20295.40	20018.63	20288.16	20626.82
8_6		20473.96	20380.93	20287.36	20446.06	20211.31	20459.88	21110.04
8_5		20607.72	20490.29	20460.34	20567.84	20395.48	20598.32	21552.29
8_4		20676.13	20636.14	20589.77	20657.85	20550.94	20739.07	21953.16
8_3		20770.85	20816.97	20709.34	20762.33	20677.08	20930.63	22310.61
8_2		20895.80	21023.51	20870.60	20902.32	20837.81	21169.35	22621.70
8_1		21044.46	21264.52	21065.87	21073.14	21041.71	21449.90	22882.58
rms[c]		1.93	36.61	16.98	20.29	18.53	137.10	682.04

[a] Notation as in ref 6, see also older data in refs 69 and 70. [b] Calculated spectra. I: From fit to experimental band positions, parameters in column "I" of Table 8. II: From fit to a 3D cut of the potential model METPOT 3, parameters in column "II" of Table 8. III: As "II", but for METPOT 4, parameters in column "III" of Table 8. IV: As "II", but for METPOT 1, parameters in column "IV" of Table 8. V: As "II", but for METPOT 1, including quasiadiabatic zero-point energies from DQMC for the frame modes, parameters in column "V" of Table 8. VI: As "II", but for a fit to a 3D cut of the model potential from ref 8 (see also footnote *a* in Table 6), parameters in column "VI" of Table 8. VII: As "II", but for a fit to a 3D cut of the model potential from ref 9, parameters in column "VII" of Table 8. [c] Root-mean-square deviation $((1/n_{dat})\sum_i^{n_{dat}}(\tilde{\nu}_{the}(i) - \tilde{\nu}_{obs}(i))^2)^{1/2}$ (all data in column $\tilde{\nu}_{obs}$).

(the root-mean-square; rms) is a shallow function of k'_{sbb}. Considering line positions and intensities, Lewerenz and Quack obtained $k'_{sbb} = 30 \pm 15$ cm^{-1}.[6]

The parameters of the chromophore potential V_{CH}^{LQ} are determined by fitting the expression eq 5 to the three-dimensional section given by eq 6. Column "II" lists the results obtained by fitting the model METPOT 3 up to energies equivalent to 20 000 cm^{-1} (three-dimensional grid with roughly 1100 points). These data correspond to an ab initio prediction of the experimental overtone spectrum, in which the equilibrium structure and harmonic force field have been refined experimentally. They show a significant improvement compared to previous results,[10,6] where the theoretical line positions were too high in relation to the experimental values, the root mean square deviation being larger by a factor of 2−5. In Table 8, the magnitudes of the parameters $K_{\rho\phi\phi}$ and $K_{\rho\rho\phi\phi}$ are smaller for the theoretical potential from eq 6 than for the experimental one (column "I"; the coefficients C_{sbb} and C_{ssbb} in dimensionless normal coordinates being larger, in magnitude, on the other hand). k'_{sbb} is approximately 50 cm^{-1} for this fit, which agrees less well with the observed intensity distribution, as will be discussed below.

Normally, when fitting the chromophore potential to experimental data, the harmonic part of V_{CH}^{LQ} is varied freely, as in column "I" of Tables 7 and 8. In fitting eq 6, the harmonic wavenumbers (e.g., ω_s and ω_b) were fixed to the values on the right-hand side to maintain a definite transformation procedure between internal and normal coordinates. To discuss this constraint, we have also fitted the experimental data by fixing the harmonic wavenumbers to the values from ref 7 (ω_b is roughly 20 cm^{-1} higher than in column "I") with the result that the root-mean-square deviation of 22 line positions is 5.7 cm^{-1} instead of 1.9 cm^{-1} from column "I". The largest deviations occur for the lowest transitions to the lowest polyads, which are shifted by roughly 10 cm^{-1} to higher values. Possible (nonexcluding) reasons for this significant discrepancy are: (A) the (quartic) force field of Gray and Robiette is approximative, the quartic order being insufficient for the description of the spectrum, including the lowest transitions, and contributions from resonance couplings need to be considered; (B) the chromophore model neglects contributions from frame modes in CHD_3 (higher than quadratic order), which may in part be compensated with an adequate variation of harmonic wavenumbers. A verification of these hypotheses is possible, in principle, with variational calculations in the complete space.

An alternative to calculate the overtone spectrum, without previous transformation of the potential surface to the V_{CH}^{LQ} form, is to directly perform (three-dimensional) variational calculations on a grid ("DVR",[26,27]). We have tested the results

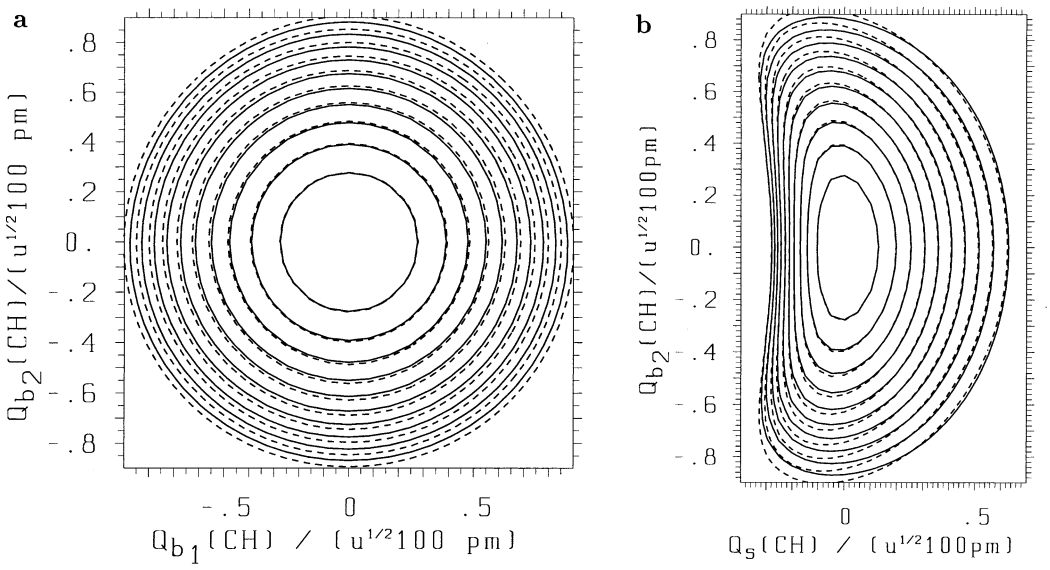

Figure 10. Equidistant potential curves of equal energy (lowest level at 2000, highest at 20 000, distance 2000 cm^{-1}). Continuous curves = METPOT 3, broken curves = METPOT 4. (a) Contour plot of the potential along Q_{b_1} and Q_{b_2}. (b) Contour plot of the potential along Q_s and Q_{b_2}.

TABLE 8: V_{CH}^{LQ} Model Potential for the CH Chromophore in CHD_3[a]: Parameter Values for Different Methane Potential Surfaces and Constants for the Effective Hamiltonian

	0	I	II	III	IV	V	VI	VII
ω_s/cm^{-1}	3128.3	3129.5	3128.0	3128.0	3128.0	3128.0	3165.0	3128.0
x_s/cm^{-1}	57.969	57.826	60.212	57.868	58.433	57.857	61.495	28.333
$K_{\phi\phi}/cm^{-1}$	56757.	56492.	58165.	58165.	58165.	57721.	60487.	56900.
$K_{\phi\phi\phi\phi}/cm^{-1}$	6418.0	8108.8	7873.5	3585.7	7376.9	3174.6	1990.6	4263.7
$K_{\rho\phi\phi}/(cm^{-1}((\mu Å^2)^{1/2})^{-1})$	−59543.	−65420.	−37584.	−40453.	−47015.	−30938.	−32841.	−49657.
$K_{\rho\rho\phi\phi}/(cm^{-1}((\mu Å^2)^{1/2})^{-2})$	97947.	112102.	27452.	38784.	44733.	100000.	29438.	43006.
$\rho_0/((\mu Å^2)^{1/2})$	1.0485	1.0485	1.0485	1.0485	1.0485	1.0485	1.0485	1.0485
$\Delta\tilde{\nu}_{fit}/cm^{-1}$ [b]	1.8	2.0	125.0	77.8	576.	318.	70.7	393.9
n_{fit}	14	22	1127	1201	286	201	1360	1269
$\Delta\tilde{V}_{conv}/cm^{-1}$ [c]	4.5	7.6	2.9	1.3	0.5	5.6	3.2	3.0
ω_b/cm^{-1}	1319.5	1316.2	1335.6	1335.6	1335.5	1330.5	1362.0	1321.0
C_{sbb}/cm^{-1}	96.8	86.5	138.7	133.4	118.4	154.9	149.6	118.5
C_{ssbb}/cm^{-1}	−50.0	−47.3	−73.7	−69.5	−65.1	−78.7	−76.5	−43.0
C_{bbbb}/cm^{-1}	−1.1	−1.6	4.1	1.4	1.7	3.4	2.4	−0.1
C_{sbbbb}/cm^{-1}	−1.3	−0.8	−7.4	−5.8	−5.2	−8.0	−7.1	−2.3
$\tilde{\nu}'_s/cm^{-1}$	3047.6	3046.9	3033.3	3042.2	3037.7	3044.2	3078.0	3078.8
$\tilde{\nu}'_b/cm^{-1}$	1292.1	1290.5	1321.0	1309.1	1315.5	1304.2	1333.6	1296.6
x'_{ss}/cm^{-1}	−58.08	−57.61	−59.44	−58.00	−56.68	−58.6	−62.21	−29.77
x'_{sb}/cm^{-1}	−21.61	−20.52	−29.16	−27.87	−28.00	−30.2	−28.94	−24.73
x'_{bb}/cm^{-1}	−4.5	−4.1	−2.8	−4.7	−3.8	−4.1	−4.7	−1.7
g'_{bb}/cm^{-1}	2.6	1.9	1.7	3.6	2.2	4.3	4.4	0.01
k'_{sbb}/cm^{-1}	25.4	16.5	48.3	45.0	30.0	52.9	61.9	104.5
$\Delta\tilde{\nu}_{eff}/cm^{-1}$ [d]	1.6	2.8	3.1	1.4	1.9	2.7	3.2	4.2

[a] V_{CH}^{LQ} defined in eq 5; parameters in column 0 are from ref 6. [b] Root-mean-square deviation from fit to n_{fit} data (all equal weights), either from experiment (line positions, columns 0 and I) or from three-dimensional cuts of the potential surfaces, as described in the text (columns II−VII). [c] Root-mean-square deviation for the conversion from polar normal coordinates into the Cartesian normal coordinates representation of V_{CH}^{LQ} on a grid $-0.4 \le Q_s/((\mu Å^2)^{1/2}) \le 1.6$ and $0.0 \le Q_b/((\mu Å^2)^{1/2}) \le 1.1$ (as explained in the text) with weighting parameter $E_{half}/hc = 10\,000\ cm^{-1}$ and maximal conversion energy equivalent to 65 000 cm^{-1} (roughly 900 points). [d] Root-mean-square deviation for the fit of the effective Hamiltonian (cf. eqs 3 and 4 in ref 6) to 48 calculated line positions (see text).

from Table 7 with such methods and found an overall agreement to within 10 cm^{-1} to up to 18 000 cm^{-1} for the present results.

The results shown in column "III" of Table 7 were obtained from the evaluation of METPOT 4. This model is the result of a "hybrid" adjustment of the potential surface representation eq 4 in paper I to the ab initio data and an additional data set of approximately 500 potential points, which stem from an experimentally determined CH chromophore potential (weighted according to eq 1 in paper I). This procedure corresponds to an experimental refinement of the model METPOT 3 with respect to the spectrum of highly excited vibrational states. These states correspond to large displacements from equilibrium and their correct calculation is therefore important for obtaining an accurate description of the underlying dynamics of large amplitude nuclear motion. Column "III" shows indeed a further, significant improvement in the description of the experimental spectrum (rms of 17 cm^{-1}). Although this spectrum does not reach the quality of the results from the direct fit of the chromophore potential model to experimental data (column "I"), it establishes a reliable description of the overtone spectrum of CHD_3 from a nine-dimensional model potential of methane.

It is interesting to note that the parameter $K_{\phi\phi\phi\phi}$ in column "III" of Table 8 is only half of its value in column "II", while all other parameters are roughly unchanged. While this seems to play an important role for the better description of experimental data, the question remains open why the parameters $K_{\phi\phi\phi\phi}$, $K_{\rho\phi\phi}$, and $K_{\rho\rho\phi\phi}$ are much smaller, in magnitude, for the ab initio determined surfaces than the corresponding values for the experimental surfaces in columns "0" and "I". A further signature of the change of $K_{\phi\phi\phi\phi}$ is that the potential surface METPOT 4 is, in general, lower in energy than METPOT 3, mainly in regions of large bending displacements. This was already observed in the foregoing graphical representations. The saddle point for the methane stereomutation is also lower in energy for METPOT 4 (see Table 1), however still in the energy region of the single CH bond rupture.

For a discussion of effects arising from the neglect of the CD_3 frame vibrations, we compare in columns "IV" and "V" results from evaluations of model METPOT 1. The first of these columns was calculated with the method described above, e.g., fitting eq 6. In column "V", we considered as the model chromophore potential the quasiadiabatic channel potential from eq 7. For CHD_3, the effect is small, as can be seen from the results in Table 7, although it accounts for a shift toward experiment for all transitions below 13 000 cm^{-1}. The quasiadiabatic interpretation might be better for compounds with relatively "heavier" CH chromphores, such as the CD group in CH_3D. A detailed analysis of this spectrum is in preparation. Other possible compounds are CHT_3 and $CM\check{u}H_3$, although not easily accessible to experiments. In ref 27, the overtone spectrum of the chiral isotopomer CMŭHDT was calculated with the model METPOT 1 (see also footnote a in Appendix 1 of paper I) and a 3D DVR calculation. This system may well be considered to be the simplest one showing a chiral symmetry-breaking anharmonic resonance of the CH chromophore. From an analysis of line positions and intensities of the theoretical spectrum, a chiral, symmetry-breaking coupling constant $k'_{sab} \approx (20 \pm 10)\ cm^{-1}$ was obtained.[27] The symbol Mŭ stands for the quasi-hydrogen isotope Mŭoniŭm (μ^+e^-).

Equation 6 may be evaluated with any general potential surface, on the right-hand side, provided it is defined in the complete vibrational space. We have also used this method to calculate the spectrum arising from the DHS[8] and LMT[9] potentials, with their corresponding harmonic force fields for the definition of normal coordinates. The overtone spectrum from the DHS potential is rather poor, when compared with experiment (column "VI"). We have also tested more recent versions of this potential,[41,42] which turned out to be even worse

in the description of the chromophore states. The LMT potential yields a spectrum that is significantly different from experiment, when transitions above 3000 cm^{-1} are considered (column "VII"). This is somewhat surprising since, from a simple comparison of the potential curves in the foregoing graphical representations (e.g., in parts a and b of Figure 2 and Figure 6a), one would expect a rather good agreement for transitions of up to at least 10 000 cm^{-1}. In the figures, the qualitative agreement of the potential curves seems to be good even at wavenumbers on the order of 20 000 cm^{-1}. A striking result is the much too low value of the stretching anharmonicity in column "VII" of Table 8. Such a finding has been reported before for the GR-potential,[10] which could be converted to the V_{CH}^{LQ} form for a maximum wavenumber of 8000 cm^{-1}, only, despite the good qualitative agreement of the potential curves shown in the previous figures.

In the conclusions of ref 6, an important result was the inclusion of integrated absorption cross sections[76]

$$G = \int_{\text{band}} \sigma(\tilde{\nu}) d \ln(\tilde{\nu}) \qquad (15)$$

in the analysis for the determination of resonance coupling constants, from which a value of (30 ± 15) cm^{-1} was finally established for k'_{sbb}. For the present fit to experiment (column "I" of Table 8), we obtain the result $k'_{sbb} \approx 17$ cm^{-1}. From the best fits to the nine-dimensional potential models, the values are closer to 50 cm^{-1}, if only line positions are considered. Within the simple CH chromophore model for intensity redistribution,[79] $k'_{sbb} \approx 50$ cm^{-1} yields an intensity distribution among the polyad states much stronger than what is observed.[6] When we formulated a more refined treatment based upon realistic models for the dipole moment operator, we saw that the intensity distribution depends sensitively on the properties of the dipole moment function, e.g., eq 1, and wave functions of the relevant states.[5,11,80] In Table 9, we have re-evaluated the integrated absorption coefficient using the dipole-moment function given in eq 1 and wave functions from the present results for the CH chromophore potential (columns "I"−"III" in Tables 7, 8, and 9). We see that, while the new "experimental" potential from column "I" yields results comparable to those from ref 11, the experimentally refined, "theoretical" potential model METPOT 4 (column "III") yields an intensity distribution which agrees even better with experiment, when the logarithmic deviations Δ_{lg} are compared. This may be related to the model dipole moment function from ref 11, which has not been adjusted here again. However, deviations from experiment data correspond to a state-of-the-art modeling of intensity distributions from nine-dimensional dipole moment functions in both cases. In column "II", the deviations are significantly larger for METPOT 3, which stresses, again, the importance of an experimental refinement procedure in the overtone region. From this discussion, we may conclude that a value for $k'_{sbb} \approx 45$ cm^{-1} is compatible with experimental results, when using a realistic model for the electric dipole moment operator, and agrees roughly with the previous findings in ref 6.

TABLE 9: Integrated Absorption Cross Sections (G_{N_j}/pm^2) of the CH Chromophore in CHD_3

	theory[a]			
N_j	I	II	III	exp
1_2	0.50×10^{-3}	0.36×10^{-2}	0.28×10^{-2}	0.10×10^{-2} [6]
1_1	0.12×10^{-0}	0.12×10^{-0}	0.12×10^{-0}	0.12×10^{-0} [6]
2_3	0.40×10^{-5}	0.12×10^{-4}	0.93×10^{-5}	
2_2	0.14×10^{-4}	0.59×10^{-4}	0.53×10^{-4}	0.90×10^{-4} [6]
2_1	0.33×10^{-3}	0.28×10^{-3}	0.32×10^{-3}	0.33×10^{-3} [6]
3_4	0.27×10^{-8}	0.27×10^{-8}	0.99×10^{-8}	
3_3	0.17×10^{-6}	0.19×10^{-5}	0.11×10^{-5}	0.23×10^{-5} [6]
3_2	0.25×10^{-5}	0.16×10^{-4}	0.13×0^{-4}	0.11×10^{-4} [6]
3_1	0.12×10^{-3}	0.11×10^{-3}	0.12×10^{-3}	0.71×10^{-4} [6]
4_3	0.27×10^{-7}	0.32×10^{-6}	0.13×10^{-6}	
4_2	0.34×10^{-6}	0.22×10^{-5}	0.14×10^{-5}	0.12×10^{-5} [6]
4_1	0.95×10^{-5}	0.80×10^{-5}	0.83×10^{-5}	0.63×10^{-5} [6]
5_4	0.02×10^{-9}	0.82×10^{-8}	0.85×10^{-9}	
5_3	0.41×10^{-8}	0.87×10^{-7}	0.24×10^{-7}	
5_2	0.59×10^{-7}	0.35×10^{-6}	0.18×10^{-6}	0.12×10^{-6} [5]
5_1	0.60×10^{-6}	0.31×10^{-6}	0.45×10^{-6}	0.71×10^{-6} [5]
6_3	0.17×10^{-8}	0.30×10^{-7}	0.67×10^{-8}	
6_2	0.17×10^{-7}	0.19×10^{-7}	0.26×10^{-7}	0.15×10^{-7} [69,72]
6_1	0.28×10^{-7}	0.15×10^{-8}	0.13×10^{-7}	0.15×10^{-7} [69,72]
7_4	0.20×10^{-9}	0.26×10^{-8}	0.32×10^{-9}	0.60×10^{-9} [72]
7_3	0.21×10^{-8}	0.10×10^{-8}	0.20×10^{-8}	0.19×10^{-8} [72]
7_2	0.14×10^{-8}	0.04×10^{-9}	0.11×10^{-8}	0.19×10^{-8} [72]
7_1	0.09×10^{-9}	0.02×10^{-9}	0.11×10^{-9}	
Δ_{lg}[e]	0.36	0.61	0.19	

[a] Values calculated with eigenvectors from columns "I", "II", and "III" of Table 8 and the dipole moment function defined in eq 1 (parameters $\mu_b^0 = 0.4$ Debye, $\mu_b^1 = -0.7000$ Debye Å^{-1}, $\mu_b^2 = -0.7744$ Debye Å^{-2}, $\mu_b^3 = -0.1079$ Debye Å^{-3}, $\beta = 0.8922$ Å^{-1}, $\mu_a^1 = 0.0570$ Debye, $\mu_a^2 = 0.0243$ Debye, $r_e = 1.0858$ Å). [e] Logarithmic deviation Δ_{lg} defined in ref 5, eq 18.

4. Conclusions

The methane potential hypersurface is among one of the most important nine-dimensional potential hypersurfaces of the smaller polyatomic molecules. It includes possibilities for prototypical reactions such as stereomutation, simple bond fission, and molecular elimination. In paper I, four slightly different model potentials for the electronic ground state of methane have been determined: METPOT 1−METPOT 4. The first two have already been referred to in our previous work.[2,3,5,11,17,81] At the moment, preference may be given for the methane model potential METPOT 4, for which the following results have been obtained, in particular, in the present work:

(1) Anharmonic zero-point energies have been obtained from the complete solution of the Schrödinger equation with the diffusion quantum Monte Carlo method (DQMC) and small statistical fluctuations,[5] which allow for a reliable determination of the experimental dissociation energy D_e within 0.4−1 kJ mol^{-1}.

(2) The equilibrium CH bond length is assumed to be 1.0858 Å, which is consistent with the previous result of Gray and Robiette.[7] The uncertainty ±0.002 Å of this value was determined here (and in ref 5), from a comparison of expectation values of effective rotational constants in the vibrational ground state, obtained with DQMC calculations, with experimental values, and is a reliable estimation of the true error bounds, which do not depend on perturbation theory.

(3) The vibrationally induced, permanent electric dipole moment in CH_3D, CH_2D_2, and CHD_3 was re-evaluated with the vector-valued, nine-dimensional dipole moment function of ref 11 and DQMC, yielding consistent results for the calculated values and the direction of the CH bond dipole moment.

(4) The calculation of vibrational transitions in the fundamental region yields, with perturbation theory, deviations from experimental data in the order of 10−20 cm^{-1}, in the test case of CH_2D_2, where perturbation theory can be applied. For METPOT 3, the anharmonic part of the potential was not further refined experimentally, and the deviations are larger (30 cm^{-1}).

(5) The overtone spectrum of the CH chromophore in CHD_3 has been obtained within a variational calculation in the three-dimensional space of the CH stretching and bending manifolds

from a completely anharmonic, nine-dimensional representation of the potential surface with an averaged deviation of 40 cm^{-1} for all observed transitions up to 18 000 cm^{-1} (METPOT 3). This may be attributed, in comparison to previous results,[10] to the experimentally refined harmonic part of the potential surface.

(6) The agreement with experimental data in the overtone spectrum of CHD_3 (line positions and intensities) may be improved a step further, with averaged deviations on the order of 15 cm^{-1}, when "experimental" potential-energy points pertaining to the experimentally determined potential surface of the CH chromophore in CHD_3 are mixed into the ab initio data set (METPOT 1, 2, and 4). Such an improvement has never been achieved before, with full-space representations of the anharmonic potential surface of methane. Remaining discrepancies may be attributed to the reduced space treatment of the CH chromophore model. A test of this hypothesis, in which the CH chromophore potential is interpreted as a quasiadiabatic effective potential, obtained with "clamped DQMC" calculations for the anharmonic zero-point energy of the frame modes, yields unaltered results, in essence.

(7) Additional improvements are possible, both by increasing the symmetry-allowed flexibility, not yet exhausted, and further optimizations of the harmonic and anharmonic parts of the potential. These may be achieved either by considering additional, more accurate ab initio energy points, e.g., from ref 9 in regions close to the equilibrium structure, or by comparison with full dimensional solutions of the Schrödinger equation for highly excited vibrational states. Such refinements should be possible, in view of the observed qualitative agreement of the model potential discussed in this work, without severe changes in the general shape of the potential energy surface, consistent with the aims established in the Introduction part of this work. In practice, new developments in variational and DVR methods[26,82−85] or quantum Monte Carlo methods[4] could be used for this purpose.

(8) In the energy range where dissociation may occur, the topography of the surface is described in a semiquantitatively correct way. The saddle point for the methane stereomutation has been described, for the first time, with a nine-dimensional analytical representation of the potential surface in a qualitatively correct manner and agrees well with results from highly specialized ab initio calculations.[47,48]

(9) Special topographical details of the potential surface can be modeled with the present nine-dimensional analytical representation. These may be of some importance for calculations of reaction rates within the several variants of scattering theories,[86,87] including statistical scattering theories[88] and possibly in real quantum scattering calculations, soon. At present, calculations with quasiadiabatic channel DQMC-methods[4] confirm the expected behavior for the effective reaction channel $CH_4 \rightarrow CH_3 + H$ from the statistical adiabatic channel model (SACM).[22] Complete calculations within the SACM are in preparation with the present, realistic methane potentials.

Acknowledgment. We enjoyed many years of friendly and fruitful scientific exchange with Fritz Schaefer. We also acknowledge help from Ioannis Thanopulos and Jürgen Stohner as well as from Marius Lewerenz and Martin Suhm in the early stages of this work. Our work is supported financially by Schweizerischer Nationalfonds and ETH-Zürich (including C4, AGS, and CSCS).

References and Notes

(1) Yamaguchi, Y.; Osamura, Y.; Goddard, J. D.; Schaefer, H. F., III. A New Dimension to Quantum Chemistry. *Analytic Derivative Methods in Ab Initio Molecular Electronic Structure Theory, The International Series of Monographs in Chemistry*; Oxford University Press: 1994; Vol. 29.

(2) Marquardt, R.; Quack, M. *Proceedomgs of the 10th International Symposium on Atomic, Molecular, Cluster, Ion, and Surface Physics, Engelberg, Switzerland*; Maier, J. P., Quack, M., Eds.; VdF Hochschulverlag: Zürich, 1996; p 19−22.

(3) Marquardt, R.; Quack, M. *J. Chem. Phys.* **1998**, *109* (24), 10628−10643.

(4) Quack, M.; Suhm, M. A. *J. Chem. Phys.* **1991**, *95* (1), 28−59.

(5) Hollenstein, H.; Marquardt, R.; Quack, M.; Suhm, M. A. *J. Chem. Phys.* **1994**, *101* (5), 3588−3602.

(6) Lewerenz, M.; Quack, M. *J. Chem. Phys.* **1988**, *88* (9), 5408−5432.

(7) Gray, D. L.; Robiette, A. G. *Mol. Phys.* **1979**, *37* (6), 1901−1920.

(8) Duchovic, R. J.; Hase, W. L.; Schlegel, H. B. *J. Phys. Chem.* **1984**, *88*, 1339−1347.

(9) Lee, T. J.; Martin, J. M. L.; Taylor, P. R. *J. Chem. Phys.* **1995**, *102* (1), 254−261.

(10) Lewerenz, M.; Marquardt, R.; Quack, M. *J. Chem. Soc., Faraday Trans. 2* **1988**, *84*, 1580−1583.

(11) Signorell, R.; Marquardt, R.; Quack, M.; Suhm, M. A. *Mol. Phys.* **1996**, *89* (1), 297−313.

(12) Schwenke, D. W.; Partridge, H. *Spectrochim. Acta* **2001**, *A57*, 887−895.

(13) Xie, J.; Tennyson, J. *Mol. Phys.* **2002**, *100* (10), 1615−1622.

(14) Xie, J.; Tennyson, J. *Mol. Phys.* **2002**, *100* (10), 1623−1632.

(15) Wang, X.-G.; Carrington, T. J. *J. Chem. Phys.* **2003**, *118* (15), 6946−6956.

(16) Wang, X.-G.; Carrington, T. J. *J. Chem. Phys.* **2003**, *119* (1), 101−117.

(17) Marquardt, R.; Quack, M.; Thanopoulos, I. *J. Phys. Chem. A* **2000**, *104* (26), 6129−6149.

(18) Marquardt, R.; Quack., M. In *Encyclopedia of Chemical Physics and Physical Chemistry*; Moore, J., Spencer, N., Eds.; IOP Publishing: Bristol, 2001; Vol. I, Chapter A3.13, pp 897−936.

(19) Suhm, M. A. Die Dynamik des Wasserstoffbrückenmoleküls $(HF)_2$: Ferninfrarotspektroskopie und Theorie Dissertation 9288, Eidgenössische Technische Hochschule Zürich, Switzerland, 1990.

(20) Blume, D.; Lewerenz, M.; Whaley, K. B. *J. Chem. Phys.* **1997**, *107* (21), 9067−9078.

(21) Quack, M.; Stohner, J.; Suhm, M. *J. Mol. Struct.* **2001**, *599*, 381−425.

(22) Quack, M.; Troe, J. *Ber. Bunsen-Ges. Phys. Chem.* **1974**, *78*, (3), 240−252.

(23) Quack, M. *J. Phys. Chem.* **1979**, *83* (1), 150−158.

(24) Quack, M.; Troe, J. In *Encyclopedia of Computational Chemistry*; Ragué Schleyer, P. v., Allinger, N., Clark, T., Gasteiger, J., Kollman, P. A., Schaefer, H. F., III, Schreiner, P. R., Eds.; John Wiley and Sons: 1998; Vol. 4, pp 2708−2726.

(25) Dübal, H.-R.; Ha, T.-K.; Lewerenz, M.; Quack, M. *J. Chem. Phys.* **1989**, *91* (11), 6698−6713.

(26) Luckhaus, D.; Quack, M. *Chem. Phys. Lett.* **1992**, *190* (6), 581−589.

(27) Beil, A.; Luckhaus, D.; Marquardt, R.; Quack, M. *J. Chem. Soc., Faraday Discuss.* **1994**, *99*, 49−76.

(28) Wilson, E. B., Jr.; Decius, J. C.; Cross, P. C. Molecular Vibrations. *The Theory of Infrared and Raman Vibrational Spectra*; McGraw-Hill Book Company, Inc.: New York, 1955.

(29) Watson, J. K. G. *Mol. Phys.* **1968**, *15* (5), 479−490.

(30) Luckhaus, D.; Quack, M. *Chem. Phys. Lett.* **1993**, *205* (2, 3), 277−284.

(31) Chase, M. W., Jr.; Davies, C. A.; Downey, J. R., Jr.; Frurip, D. J.; McDonald, R. A.; Syverud, A. N. *JANAF Thermochemical Tables, J. Phys. Chem. Ref. Data*, 3rd ed.; American Chemical Society and American Institute of Physics for the National Bureau of Standards, 1985; Vol. 14, Suppl. 1.

(32) Berkowitz, J.; Ellison, G. B.; Gutman, D. *J. Phys. Chem.* **1994**, *98*, 8 (11), 2744−2765.

(33) Weitzel, K.-M.; Malow, M.; Jarvis, G. K.; Baer, T.; Song, Y.; Ng, C. Y. *J. Chem. Phys.* **1999**, *111*, 8267−8271.

(34) Kelly, P. B.; Westre, S. G. *Chem. Phys. Lett.* **1988**, *151* (3), 253−257.

(35) Miller, J. T.; Burton, K. A.; Weisman, R. B.; Wu, W.-X.; Engel, P. S. *Chem. Phys. Lett.* **1989**, *158* (3, 4), 179−183.

(36) Lewerenz, M. Potential und Dynamik des CH Chromophors in CD_3H: Hochauflösende Spektroskopie und ab initio Berechnungen Diploma Thesis, Universität Bonn, 1983.

(37) Yamada, C.; Hirota, E.; Kawaguchi, K. *J. Chem. Phys.* **1981**, *75* (11), 5256−5364.

(38) Cobos, C. J.; Troe, J. *Chem. Phys. Lett.* **1985**, *113* (5), 419−424.

(39) Duchovic, R. J.; Hase, W. L. *J. Chem. Phys.* **1985**, *82* (8), 3599−3606.

(40) Hase, W. L.; Duchovic, R. J. *J. Chem. Phys.* **1985**, *83* (7), 3448−3453.
(41) Hase, W. L.; Mondro, S. L.; Duchovic, R. J.; Hirst, D. M. *J. Am. Chem. Soc.* **1987**, *109*, 2916−2922.
(42) Hu, X.; Hase, W. L. *J. Chem. Phys.* **1991**, *95* (11), 8073−8082.
(43) LeBlanc, J. F.; Pacey, P. D. *J. Chem. Phys.* **1985**, *83*, 4511−4515.
(44) Brouard, M.; Macpherson, M. T.; Pilling, M. J.; Tulloch, J. M.; Williamson, A. P. *Chem. Phys. Lett.* **1985**, *113* (5), 413−418.
(45) Quack, M. *Il Nuovo Cimento* **1981**, *63B*, 358−377.
(46) Peyerimhoff, S.; Lewerenz, M.; Quack, M. *Chem. Phys. Lett.* **1984**, *109* (6), 563−569.
(47) Gordon, M. S.; Schmidt, M. W. *J. Am. Chem. Soc.* **1993**, *115*, 7486−7492.
(48) Pepper, M. J. M.; Shavitt, I.; Ragué Schleyer, P. v.; Glukhovtsev, M. N.; Janoschek, R.; Quack, M. *J. Comput. Chem.* **1995**, *16* (2), 207−225.
(49) McCarthy, M. I.; Rosmus, P.; Werner, H.-J.; Botschwina, P.; Vaida, V. *J. Chem. Phys.* **1987**, *86* (12), 6693−6700.
(50) Hirst, D. M. *Chem. Phys. Lett.* **1985**, *122* (3), 225−229.
(51) Baer, T.; Hase, W. L. Unimolecular Reaction Dynamics. *Theory and Experiment*; Oxford University Press: New York, Oxford, 1996.
(52) Banerjee, A.; Adams, N.; Simons, J.; Shepard, R. *J. Phys. Chem.* **1985**, *89*, 52−57.
(53) Bunker, P. R.; Jensen, P.; Kraemer, W. P.; Beardsworth, R. *J. Chem. Phys.* **1986**, *85* (7), 3724−3731.
(54) Bunker, P. R.; Kraemer, W. P.; Špirko, V. *J. Mol. Spectrosc.* **1983**, *101*, 180−185.
(55) Bauschlicher, C. W.; Haber, K.; Schaefer, H. F., III; Bender, C. F. *J. Am. Chem. Soc.* **1977**, *99* (11), 3610−3614.
(56) Kollmar, H.; Staemmler, V. *Theor. Chim. Acta* **1979**, *51*, 207−217.
(57) Baskin, C. P.; Bender, C. F.; Bauschlicher, C. W., Jr.; Schaefer, H. F., III. *J. Am. Chem. Soc.* **1974**, *96* (9), 2709−2713.
(58) Quack, M.; Suhm, M. A. In *Conceptual Perspectives in Quantum Chemistry*; Calais, J.-L., Kryachko, E. S., Eds.; Kluwer Academic Publishers: Dordrecht, 1997; Vol. III, pp 417−465.
(59) Anderson, J. B. *J. Chem. Phys.* **1975**, *63* (4), 1499−1503.
(60) Papousek, D.; Aliev, M. R. *Molecular Vibrational−Rotational Spectra*; Elsevier Scientific Publishing Company: Amsterdam, 1982.
(61) Grev, R. S.; Janssen, C. L.; Schaefer, H. F., III *J. Chem. Phys.* **1991**, *99* (7), 5128−5132.
(62) Pulay, P.; Fogarasi, G.; Pang, F.; Boggs, J. E. *J. Am. Chem. Soc.* **1979**, *101* (10), 2550−2560.
(63) Siegbahn, P. E. M. *Chem. Phys. Lett.* **1985**, *119* (6), 515−521.
(64) Bowen-Jenkins, P.; Pettersson, L. G. M.; Siegbahn, P.; Almlöf, J.; Taylor, P. R. *J. Chem. Phys.* **1988**, *88* (11), 6977−6981.
(65) Partridge, H.; Bauschlicher, C. W., Jr. *J. Chem. Phys.* **1995**, *103* (24), 10589−10596.
(66) Duncan, J. L.; Mills, I. M. *Spectrochim. Acta* **1964**, *20*, 523−546.
(67) Carrington, T., Jr.; Halonen, L.; Quack, M. *Chem. Phys. Lett.* **1987**, *140*(5), 512−519.
(68) Iung, C.; Leforestier, C. *J. Chem. Phys.* **1989**, *90* (6), 3198−3203.
(69) Scherer, G. J.; Lehmann, K. K.; Klemperer, W. *J. Chem. Phys.* **1984**, *81* (12), 5319−5325.
(70) Perry, J. W.; Moll, D. J.; Kuppermann, A.; Zewail, A. H. *J. Chem. Phys.* **1985**, *82* (3), 1195−1211.
(71) Campargue, A.; Stoeckel, F. *J. Chem. Phys.* **1986**, *85* (3), 1220−1227.
(72) Ben Kraiem, H.; Campargue, A.; Chenevier, M.; Stoeckel, F. *J. Chem. Phys.* **1989**, *91* (4), 2148−2152.
(73) Permogorov, D.; Campargue, A.; Chenevier, M.; Ben Kraiem, H. *J. Mol. Spectrosc.* **1995**, *170*, 10−26.
(74) Dupre-Maquaire, J. *J. Mol. Spectrosc.* **1983**, *101*, 319−324.
(75) Campargue, A.; Stoeckel, F.; Chenevier, M.; Ben Kraiem, H. *J. Chem. Phys.* **1987**, *87* (10), 5598−5605.
(76) Quack, M. *Annu. Rev. Phys. Chem.* **1990**, *41*, 839−874.
(77) Domingo, C.; del Olmo, A.; Escribano, R.; Bermejo, D.; Orza, J. M. *J. Chem. Phys.* **1992**, *96* (2), 972−975.
(78) Marquardt, R.; Gonçalves, N. S.; Sala, O. *J. Chem. Phys.* **1995**, *103* (19), 8391−8403.
(79) Dübal, H.-R.; Quack, M. *J. Chem. Phys.* **1984**, *81* (9), 3779−3791.
(80) Ha, T.-K.; Lewerenz, M.; Marquardt, R.; Quack, M. *J. Chem. Phys.* **1990**, *93* (10), 7097−7109.
(81) Hollenstein, H.; Marquardt, R. R.; Quack, M.; Suhm, M. A. *Ber. Bunsen-Ges. Phys. Chem.* **1995**, *99*, 9 (3), 275−281.
(82) Bramley, M. J.; Carrington, T. *J. Chem. Phys.* **1993**, *99* (11), 8519−8541.
(83) Jungwirth, P.; Gerber, R. B. *J. Chem. Phys.* **1995**, *102* (22), 8855−8864.
(84) Iung, C.; Leforestier, C. *J. Chem. Phys.* **1994**, *102* (21), 8453−8461.
(85) Maynard, A. T.; Wyatt, R. E.; Iung, C. *J. Chem. Phys.* **1995**, *103* (19), 8372−8390.
(86) Truhlar, D. G.; Garrett, B. C.; Klippenstein, S. J. *J. Phys. Chem.* **1996**, *100* (31), 12771−12800.
(87) Schatz, G. C. *J. Phys. Chem.* **1996**, *100* (31), 12839−12847.
(88) Quack, M.; Troe, J. *Theor. Chem.: Adv. Perspect.* **1981**, *6B*, 199−276.
(89) Champion, J. P.; Hilico, J. C.; Brown, L. R. *J. Mol. Spectrosc.* **1989**, *133*, 244−256.
(90) Tarrago, G.; Delaveau, M.; Fusina, L.; Guelachvili, G. *J. Mol. Spectrosc.* **1987**, *126*, 149−158.
(91) Ulenikov, O. N.; Malikova, A. B.; Shevchenko, G. A.; Guelachvili, G.; Morillon-Chapey, M. *J. Mol. Spectrosc.* **1991**, *149*, 160−166.
(92) Tarrago, G.; Dupre-Maquaire, J. *J. Mol. Spectrosc.* **1982**, *96*, 170−174.
(93) Lolck, J.-E.; Poussigue, G.; Pascaud, E.; Guelachvili, G. *J. Mol. Spectrosc.* **1985**, *111*, 235−274.
(94) Ulenikov, O. N.; Malikova, A. B.; Guelachvili, G.; Morillon-Chapey, M. *J. Mol. Spectrosc.* **1993**, *159*, 422−436.
(95) Ulenikov, O. N.; Tolchenov, R. N.; Koivusaari, M.; Alanko, S.; Anttila, R. *J. Mol. Spectrosc.* **1994**, *167*, 109−130.